

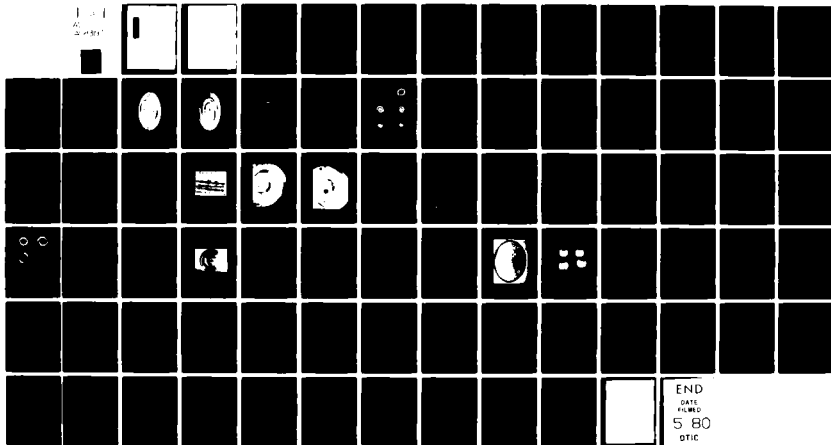
AD-A083 197

DAVID W TAYLOR NAVAL SHIP RESEARCH AND DEVELOPMENT CE--ETC F/8 13/7  
INVESTIGATION OF THE SCROLL MECHANISM FOR PUMPING HYDRAULIC FLU--ETC(U)  
MAR 80 T W BEIN, M A BERGMAN

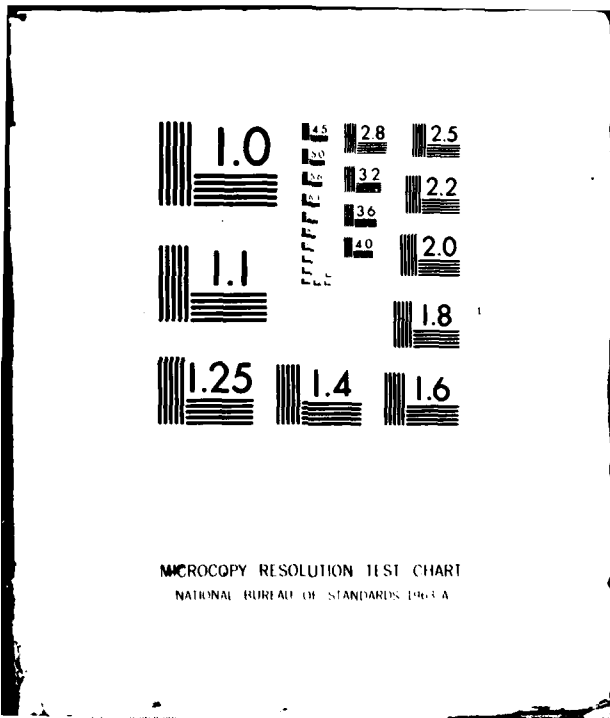
UNCLASSIFIED

NL

1-1  
2-1

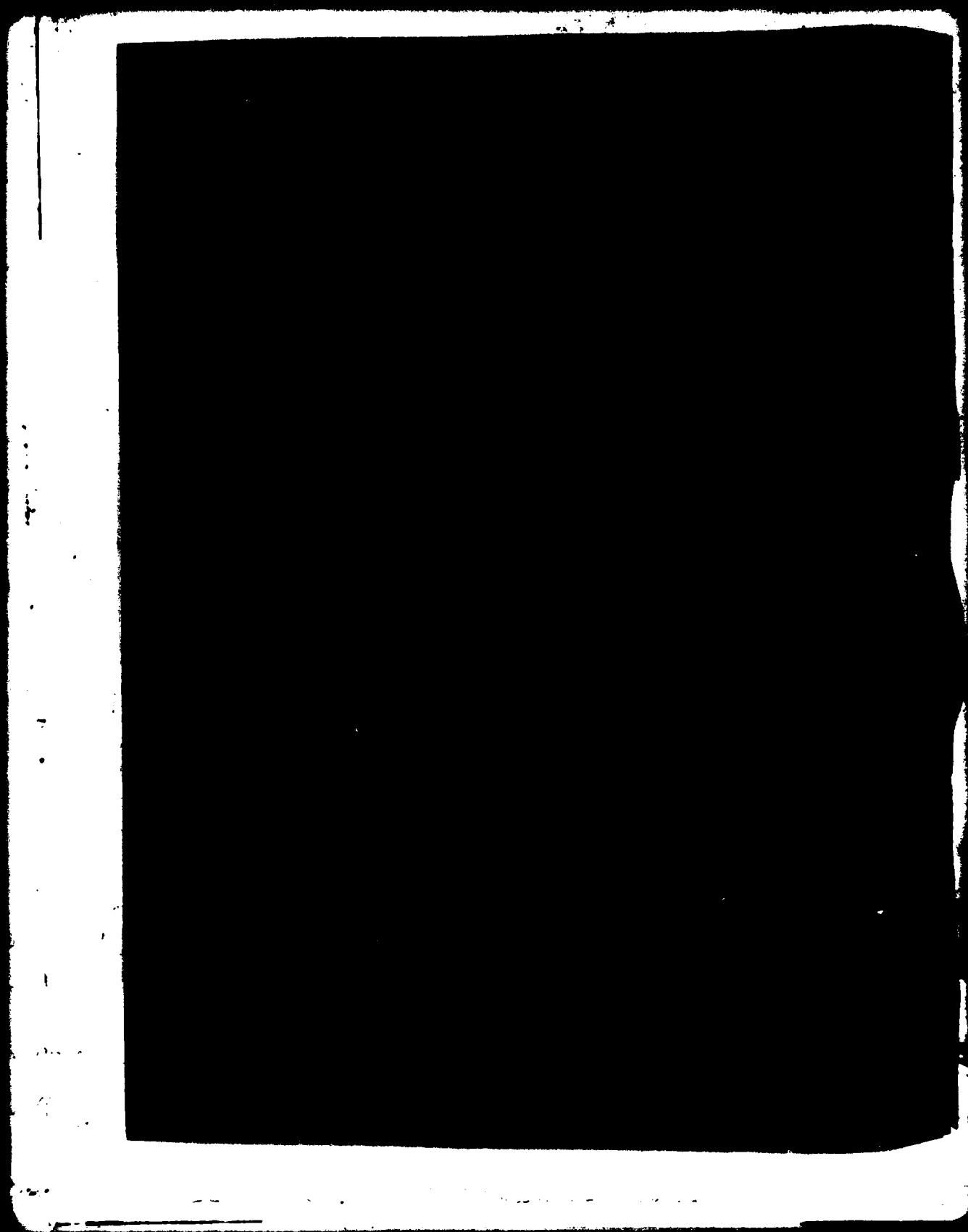


END  
DATE  
FILMED  
5 80  
DTIC



MICROCOPY RESOLUTION TEST CHART  
NATIONAL BUREAU OF STANDARDS 1963-A

ADA 083197



UNCLASSIFIED

SECURITY CLASSIFICATION OF THIS PAGE (When Data Entered)

REPORT DOCUMENTATION PAGE		READ INSTRUCTIONS BEFORE COMPLETING FORM
1. REPORT NUMBER DTNSRDC-80/031	2. GOVT ACCESSION NO.	3. RECIPIENT'S CATALOG NUMBER
6. INVESTIGATION OF THE SCROLL MECHANISM FOR PUMPING HYDRAULIC FLUID		4. TYPE OF REPORT & PERIOD COVERED Final rept.
7. AUTHOR(s) Thomas W. Bein Mark A. Bergman		5. PERFORMING ORG. REPORT NUMBER
8. PERFORMING ORGANIZATION NAME AND ADDRESS David W. Taylor Naval Ship R&D Center Annapolis, MD 21402		9. CONTRACT OR GRANT NUMBER(s)
11. CONTROLLING OFFICE NAME AND ADDRESS David W. Taylor Naval Ship R&D Center Bethesda, MD 20084		10. PROGRAM ELEMENT, PROJECT, TASK AREA & WORK UNIT NUMBERS Prog. Element 62766N Task Area Z-F61-512-001 Work Unit 1-2703-100
14. MONITORING AGENCY NAME & ADDRESS (if different from Controlling Office)		12. REPORT DATE March 1980
12. 79		13. NUMBER OF PAGES 78
16. DISTRIBUTION STATEMENT (of this Report) APPROVED FOR PUBLIC RELEASE; DISTRIBUTION UNLIMITED		18. SECURITY CLASS. (of this report) UNCLASSIFIED
16. F61512 17. ZF61512001		19a. DECLASSIFICATION/DOWNGRADING SCHEDULE
17. DISTRIBUTION STATEMENT (for the abstract entered in Block 20, if different from Report)		
18. SUPPLEMENTARY NOTES		
19. KEY WORDS (Continue on reverse side if necessary and identify by block number) Hydraulic Pumps Scroll Involute (20,700,000 Pa)		
20. ABSTRACT (Continue on reverse side if necessary and identify by block number) Two 3000-psi ( $2.07 \times 10^7$ Pa) hydraulic pumps, designed using the principles of the scroll mechanism, were built and evaluated to determine their feasibility for future shipboard hydraulic service. This report presents the geometry, mathematical models, and machining techniques required to fabricate these prototypes. The first-generation pump demonstrated a 95 percent volumetric efficiency at 500 psi ( $3.4 \times 10^6$ Pa), while the improved (Continued on reverse side)		

DD FORM 1 JAN 73 1473

EDITION OF 1 NOV 65 IS OBSOLETE  
S/N 0102-LF-014-6601

UNCLASSIFIED

SECURITY CLASSIFICATION OF THIS PAGE (When Data Entered)

(34,000,000 Pa)

387682

Jim

UNCLASSIFIED

SECURITY CLASSIFICATION OF THIS PAGE (When Data Entered)

(Block 20 continued)

→ synchronously rotating drive mechanism of the second-generation unit eliminated the vibration and balance problems of the first-generation orbiting drive arrangement. This report also presents recommendations for follow-on scroll pump work. However, based on the results to date, the program has been suspended, pending evaluation of other Navy pump concepts. ←

Accession For  
Navy G.I.  
DDC Tag  
Unannounced  
Justification  
By  
Date  
Approved for  
Dist A  
Special

UNCLASSIFIED

SECURITY CLASSIFICATION OF THIS PAGE (When Data Entered)

TABLE OF CONTENTS

	Page
LIST OF FIGURES . . . . .	iv
TABLE . . . . .	v
NOTATION. . . . .	vii
LIST OF ABBREVIATIONS . . . . .	ix
ABSTRACT. . . . .	1
ADMINISTRATIVE INFORMATION. . . . .	1
INTRODUCTION. . . . .	1
BACKGROUND . . . . .	1
SCOPE. . . . .	2
APPROACH . . . . .	2
DESCRIPTION OF PROTOTYPE--FIRST-GENERATION PUMP . . . . .	2
BASIC DESIGN . . . . .	2
FABRICATION. . . . .	9
TEST PROCEDURE--FIRST-GENERATION PUMP . . . . .	9
SYSTEM DESCRIPTION . . . . .	9
INSTRUMENTATION. . . . .	11
OPERATION. . . . .	13
RESULTS--FIRST-GENERATION PUMP. . . . .	13
DISCUSSION--FIRST-GENERATION PUMP . . . . .	15
DESCRIPTION OF PROTOTYPE--SECOND-GENERATION PUMP. . . . .	28
BASIC DESIGN . . . . .	28
FABRICATION. . . . .	31
TEST PROCEDURE--SECOND-GENERATION PUMP. . . . .	31
SYSTEM DESCRIPTION . . . . .	31
INSTRUMENTATION. . . . .	34
OPERATION. . . . .	34

	Page
RESULTS--SECOND-GENERATION PUMP . . . . .	34
DISCUSSION--SECOND-GENERATION PUMP. . . . .	40
CONCLUSIONS AND RECOMMENDATIONS . . . . .	42
SCROLL PLATES. . . . .	42
DRIVE METHOD . . . . .	44
MEASUREMENTS . . . . .	44
ACKNOWLEDGMENTS . . . . .	44
APPENDIX A - SCROLL GEOMETRIC RELATIONSHIPS . . . . .	45
APPENDIX B - LEAKAGE PAST THE FLANK OF THE SCROLL VANES . . . . .	53
REFERENCES. . . . .	67

LIST OF FIGURES

1 - Stationary Scroll Plate--First-Generation Pump . . . . .	4
2 - Moving Scroll Plate--First-Generation Pump . . . . .	5
3 - Cutaway of First-Generation Pump . . . . .	6
4 - Pocket Progression--Orbiting Drive . . . . .	8
5 - Scroll Piping Schematic--First-Generation Pump . . . . .	10
6 - Position of Strain Gages on Oldham Ring--First-Generation Pump . . . . .	12
7 - Static Leakage Test--First-Generation Pump . . . . .	14
8 - Effect of Pressure Behind Moving Scroll Plate on Volumetric Efficiency--First-Generation Pump. . . . .	16
9 - Volumetric Efficiency--First-Generation Pump . . . . .	17
10 - Overall Efficiency--First-Generation Pump. . . . .	18
11 - Torque Applied to Oldham Ring--First-Generation Pump . . . . .	19
12 - Damaged Moving Scroll Plate--First-Generation Pump . . . . .	20



	Page
13 - Damaged Stationary Scroll Plate--First-Generation Pump . . . . .	21
14 - Predicted Volumetric Efficiency for Various Flank Clearances with Tip Clearance = 0.0 in.--First-Generation Pump. . . . .	23
15 - Predicted Volumetric Efficiency for Various Tip Clearances with Flank Clearance = 0.0 in.--First-Generation Pump. . . . .	24
16 - Comparison of Actual and Projected Volumetric Efficiencies . .	25
17 - Axial Forces on the Moving Scroll Plate--First-Generation Pump . . . . .	27
18 - Cutaway of Second-Generation Pump. . . . .	29
19 - Pocket Progression--Synchronously Rotating Drive--Second- Generation Pump. . . . .	30
20 - Pocket Volume Progression--Synchronously Rotating Drive-- Second-Generation Pump . . . . .	32
21 - Driver Scroll Plate--Second-Generation Pump. . . . .	33
22 - Occurrence of Large Pressure Fluctuations--Second- Generation Pump. . . . .	36
23 - Volumetric Efficiency at Points Where Pressure Fluctuations Occurred--Second-Generation Pump . . . . .	37
24 - Damaged Oldham Ring--Second-Generation Pump. . . . .	38
25 - Damaged Oldham Ring Guides--Second-Generation Pump . . . . .	39
26 - Axial Forces on the Driver Scroll Plate--Second-Generation Pump . . . . .	41
27 - Predicted Volumetric Efficiencies at 3000 psi (2.07 x 10 <sup>7</sup> Pa) Discharge--First-Generation Pump . . . . .	43
28 - Basic Geometry . . . . .	46
29 - Scroll Phase Angles. . . . .	47
30 - Differential Involute Area . . . . .	49

	Page
31 - Area of a Pocket . . . . .	51
32 - Gap Between Scroll Sides . . . . .	55

TABLE

1 - Prototype Scroll Hydraulic Pump Design Data. . . . .	3
--	---

## NOTATION

AB	Length of line tangent to the generating circle to a point on involute = $r_g \theta$
$A_G$	Area of gap
$A_I$	Area of involute
$A_P$	Area of pocket
D	Hydraulic diameter
f	Friction factor
$g_c$	Dimensional conversion factor
GAP	Distance between sides of two vanes
H	Height of scroll vanes
$H_L$	Head loss
L	Length of perimeter of an involute
$N_V$	Number of vanes on a plate
P	Pressure
R	Defined as = $r_g \theta_1 \pi$
$r_g$	Generating radius
$r_o$	Orbiting radius = $r_g \gamma$
t	Vane thickness = $r_g \phi$
V	Velocity
w	Flowrate through gap between scroll vanes
X	Defined as = $\theta R$
Y	Total distance between vane sides = gap + $Y_o$

$Y_o$	Side clearance between two vanes
Z	Length of line tangent to the generating circle to a point on an involute = $r_g \theta$
$\beta_{IE}$	Angle of inner sealing surface at the end of the pocket
$\beta_{IS}$	Angle of inner sealing surface at the start of the pocket
$\beta_{OE}$	Angle of outer sealing surface at the end of the pocket
$\beta_{OS}$	Angle of outer sealing surface at the start of the pocket
$\gamma$	Angle between mating scroll surfaces = $\alpha - \phi$
$\alpha$	Phase angle between scroll plates = $\pi/N_v$
$\phi$	Angle between the starting axis of the edges of a vane
$\theta$	Angular position
$\rho$	Density
$\mu$	Absolute viscosity

## LIST OF ABBREVIATIONS

cm <sup>2</sup>	Square centimeter
cm <sup>3</sup>	Cubic centimeter
deg	Angular degree
F	Degree Fahrenheit
hp	Horsepower
in.	Inch
in. <sup>2</sup>	Square inch
in. <sup>3</sup>	Cubic inch
kW	Kilowatt
mm	Millimeter
Pa	Pascal
psi	Pound per square inch
rpm	Revolution per minute
µm	Micrometer

## ABSTRACT

Two 3000-psi ( $2.07 \times 10^7$  Pa) hydraulic pumps, designed using the principles of the scroll mechanism, were built and evaluated to determine their feasibility for future shipboard hydraulic service. This report presents the geometry, mathematical models, and machining techniques required to fabricate these prototypes. The first-generation pump demonstrated a 95 percent volumetric efficiency at 500 psi ( $3.4 \times 10^6$  Pa), while the improved synchronously rotating drive mechanism of the second-generation unit eliminated the vibration and balance problems of the first-generation orbiting drive arrangement. This report also presents recommendations for follow-on scroll pump work. However, based on the results to date, the program has been suspended, pending evaluation of other Navy pump concepts.

## ADMINISTRATIVE INFORMATION

This work was accomplished under Independent Exploratory Development funding, Task Area Z-F61-512-001. The Work Unit number was 1-2703-100.

## INTRODUCTION

### BACKGROUND

The Navy is engaged in ongoing programs to increase the operating efficiency and performance of its shipboard auxiliary equipment. A mathematical analysis of a scroll pump concept shows it to have good potential as a high volumetric-efficiency, high-pressure pump. An attractive shipboard application of the scroll mechanism is as a 3000-psi ( $2.07 \times 10^7$  Pa), positive displacement, hydraulic pump having few moving parts. The scroll pump would be quieter and have less fluid pulsation because its discharge flowrate is nearly constant. Also, the required critical clearances of such a pump would tend to diminish as the scrolls wear in, instead of increasing as in conventional pumps. Hence, the volumetric efficiency of the scroll pump should remain high as a function of time.

## SCOPE

This report covers the design, fabrication, evaluation, and development of two prototype scroll hydraulic pumps.

## APPROACH

The general geometric relationships used in the design of scroll mechanisms are presented in Appendix A. Mathematical predictions were made on the pressures, flowrates, and loads in the pump. Based on these design predictions, two prototype pumps were built and experimentally evaluated. The design data used for each of the prototypes is given in Table 1. The investigation of the two pump designs (first-generation and second-generation) are reported separately. However, the conclusions and recommendations are based on the information from both pumps.

## DESCRIPTION OF PROTOTYPE--FIRST-GENERATION PUMP

### BASIC DESIGN

Figures 1 and 2 show the involute vanes on the stationary scroll plate and the moving scroll plate of the first-generation pump. The moving scroll plate travels in an orbiting motion about the center of the stationary plate. An Oldham ring is used to allow the moving plate to orbit but to prevent it from rotating about its own center. A crankpin that is eccentrically mounted to the drive shaft drives the moving scroll plate via bearings (Figure 3). The drive shaft and the stationary scroll plate are positioned on the same centerline; hence, the orbiting radius is the distance from the center of the drive shaft to the center of the offset crankpin. A counterweight on the drive shaft balances the moving scroll plate. The secondary moments are not balanced, nor is the Oldham ring. Because the drive shaft is in a high-pressure area, a labyrinth seal on the shaft drops the pressure so that a low-pressure, mechanical face seal can be used where the shaft goes through the case.

TABLE 1 - PROTOTYPE SCROLL HYDRAULIC PUMP DESIGN DATA

Description	First-Generation Pump	Second-Generation Pump
Generating radius	0.326 in. (8.28 mm)	0.237 in. (6.02 mm)
Orbiting radius	0.142 in. (3.61 mm)	0.372 in. (9.45 mm)
Number of vanes per plate	2	1
Number of pockets	4	2
Width of vane	0.369 in. (9.37 mm)	0.372 in. (9.45 mm)
Phase angle between plages	90 deg	180 deg
Angle of outside contact on inside scroll vane	471 deg	590 deg
Single pocket area	1.540 in. <sup>2</sup> (9.94 cm <sup>2</sup> )	4.40 in. <sup>2</sup> (28.38 cm <sup>2</sup> )
Height of vanes	0.240 in. (6.10 mm)	0.252 in. (6.40 mm)
Single pocket volume	0.370 in. <sup>3</sup> (6.06 cm <sup>3</sup> )	1.109 in. <sup>3</sup> (18.17 cm <sup>3</sup> )
Displacement per revolution	1.480 in. <sup>3</sup> (24.25 cm <sup>3</sup> )	2.218 in. <sup>3</sup> (36.35 cm <sup>3</sup> )
Scroll Plate Material:		
Moving - Driver	HY tool steel	Nodular cast iron
Stationary - Driven	Low carbon steel	Nodular cast iron





Figure 1 - Stationary Scroll Plate -- First-Generation Pump

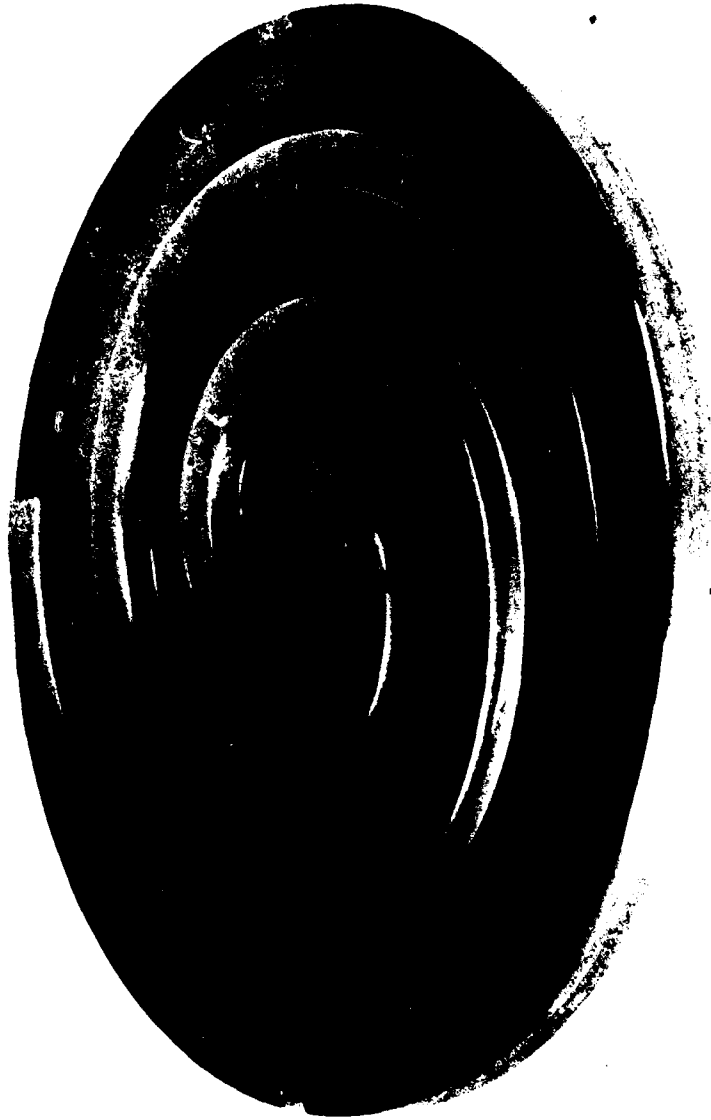


Figure 2 - Moving Scroll Plate -- First-Generation Pump

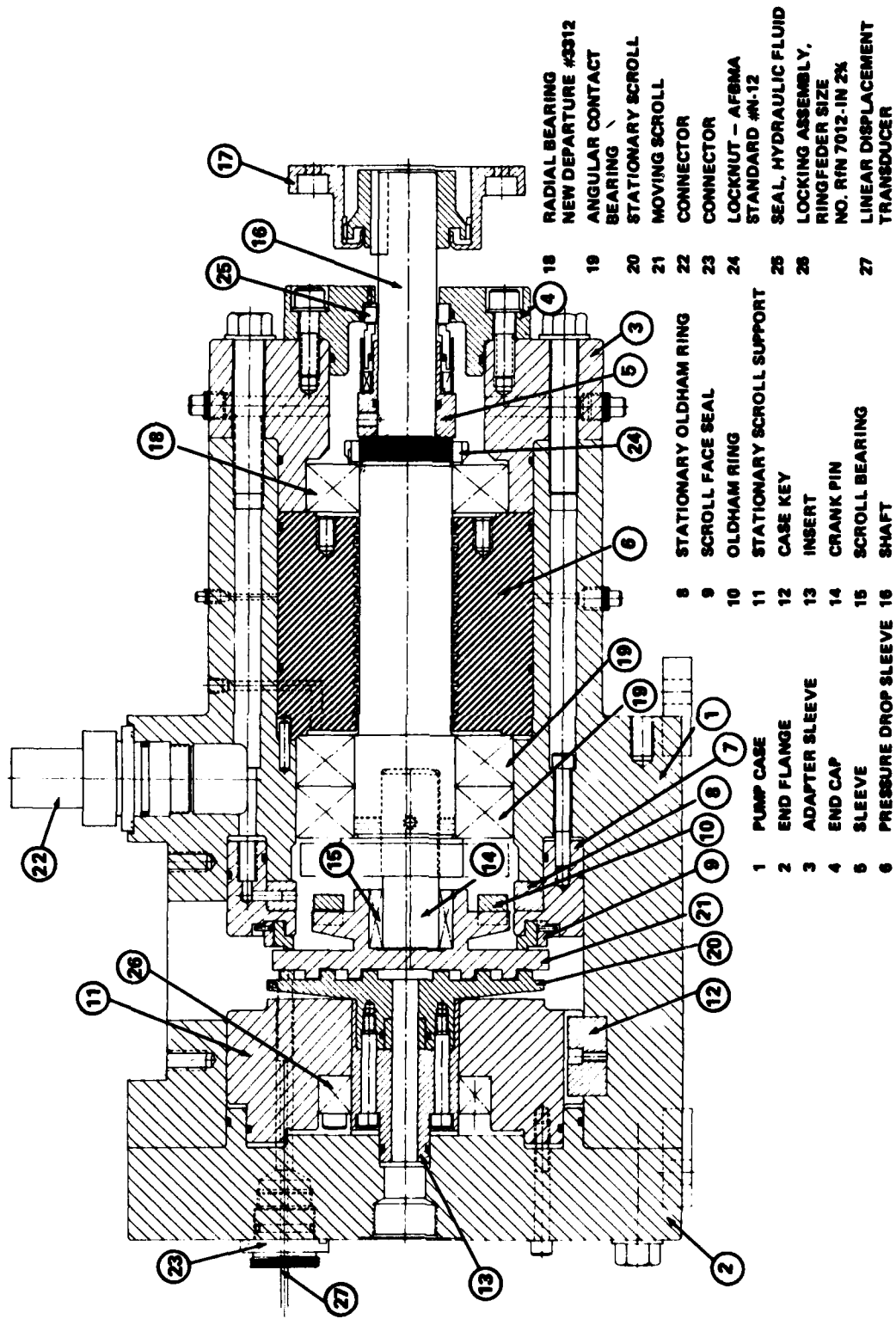


Figure 3 - Cutaway of First-Generation Pump

The area around the outside diameter of the scroll plates is the suction chamber. Figure 4 shows the basic pumping cycle. Liquid begins the pumping cycle (A), when it enters a pocket created between two scroll vanes. When the pocket is full, a contact point between the two scroll vanes is established at the outer edge at the same time the contact point at the inner edge opens (B). The outer contact point then progresses toward the center (C, D, E). The volume of the pocket diminishes as the contact point moves toward the center, thereby delivering the liquid that was contained in the pocket. When all of the liquid has been delivered, the sealing point opens and the cycle repeats. The liquid discharges through a hole in the center of the stationary plate.

The moving scroll plate is free to move axially so that it is able to compensate for wear of the two scroll plates. The moving scroll plate is pushed toward the stationary scroll plate by pressurizing the area behind the moving scroll plate. A mechanical face seal seals against the back side of the moving scroll plate and prevents the high-pressure fluid behind the plate from leaking into the suction chamber. From the mathematical analysis of the scroll pumping cycle it was found that, when the inner contact point opens and the liquid contained in the pocket begins to discharge, the rate of change of the pocket volume is greater than the volume that can pass through the discharge opening. While this problem only lasts for a small part of the cycle, it results in severe over-pressurization during that time. The additional loading that results causes inefficiencies and probable mechanical damage to the pump. This problem was solved<sup>1</sup> by providing an additional discharge port. At the time that the normal discharge port begins to slowly open, the additional discharge port opens rapidly and provides a discharge area many times greater than the area of the normal discharge port operating alone. These additional discharge ports are visible in Figures 1 and 2. Liquid is transferred from the pocket into the "T" shaped slots in a vane and into the center discharge area.

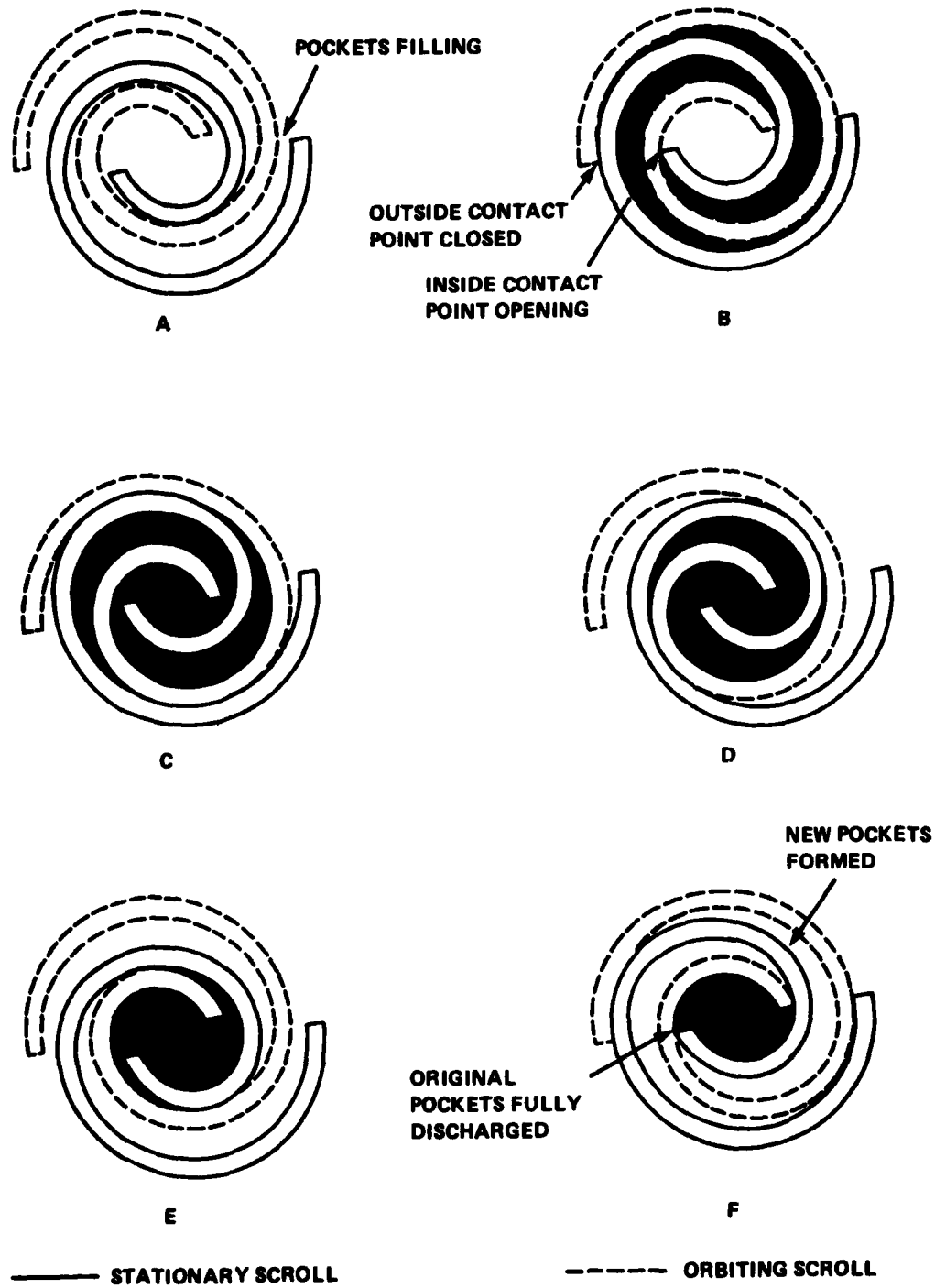


Figure 4 - Pocket Progression -- Orbiting Drive

## FABRICATION

Conventional machining techniques were used for all of the components except the scroll plates. These were machined on a numerically controlled milling machine that could not blend the X and Y coordinates. As a result the flanks of the scroll vanes had small steps in them. After machining, the set of scroll plates were put into a lapping fixture that held the plates in the proper position while it was in operation. During the lapping procedure, the correct angular position (referred to as the phase angle and described in Appendix A) between the two scroll plates was determined and marked so that the plates would be put into the same position when installed into the pump housing. Lapping was continued until the plates showed a wear pattern of full contact between them. The steps in the flanks of the scroll vanes were also lapped smooth.

After lapping, the moving scroll plate was balanced by placing it and the drive shaft as an assembly into the balancing machine. As previously mentioned, the secondary moments were not balanced.

## TEST PROCEDURE--FIRST-GENERATION PUMP

### SYSTEM DESCRIPTION

A piping schematic of the pump installation is shown in Figure 5. A brief description of the diagram follows:

The receiver tank holds approximately eighty gallons of type 2190 turbine oil and is kept under a pressure of 25 to 40 psi ( $1.7$  to  $2.5 \times 10^5$  Pa) by the nitrogen bottle (F). A 25  $\mu$ m filter filters all oil leaving the receiver tank. An auxiliary pump (A) provides pressure behind the moving plate at start up. Once the scroll develops sufficient discharge pressure the three-way valve (5) is positioned to provide pressure behind the moving plate from the discharge line. At that time, the auxiliary pump can be valved out of the system. A needle valve (8) regulates the pressure behind the moving plate.

An accumulator (C) is connected to the discharge line to dampen pulsations in the fluid flow and a relief valve (D) protects against overpressurization of the discharge line. A 10  $\mu$ m filter in the

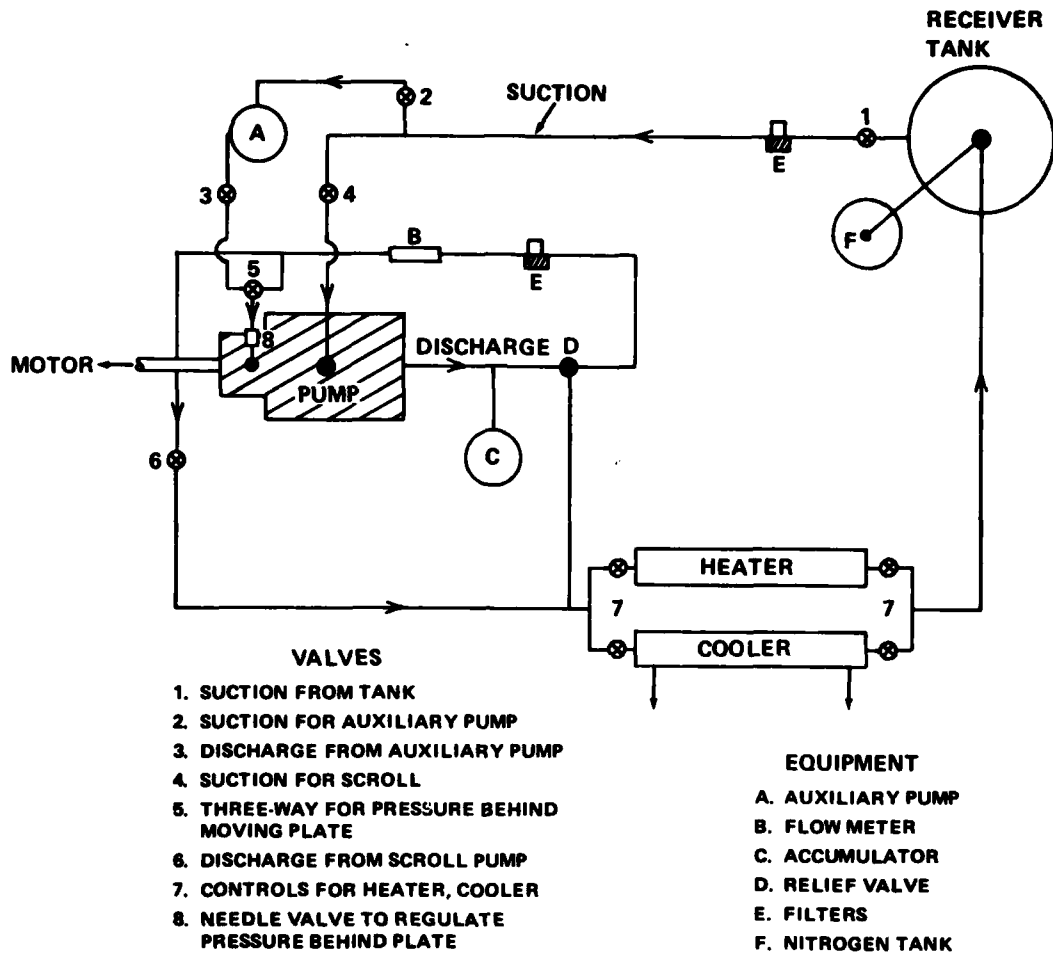


Figure 5 - Scroll Piping Schematic -- First-Generation Pump

discharge line protects the turbine-type flow meter from particle damage. Discharge pressure is controlled by a throttling valve (6). The oil then passes through either a heater or cooler, as necessary, to keep the oil between 95 F and 105 F (35 C to 41 C).

Power to drive the pump is provided by a 900 rpm - 25 hp (18.7 kW) ac motor.

#### INSTRUMENTATION

Transducers were used during testing to determine pressure at the following points:

1. discharge pressure immediately out of the case
2. pressure behind the moving plate
3. suction pressure at the inlet
4. receiver tank pressure
5. pressure in the shaft seal area

The various temperatures monitored with thermocouples were:

1. discharge temperature of the oil
2. suction temperature of the oil
3. oil temperature in the rear cavity of the pump
4. oil temperature in the shaft seal
5. oil entering and leaving the heat exchangers

A rotary transformer torque transducer measured the input shaft torque and rpm.

A turbine-type flow meter measured the flow rate in the discharge line.

Strain gages were placed on the Oldham ring as shown in Figure 6 to determine the magnitude and direction of the torque applied to the ring.

A linear voltage displacement transducer was used to determine the distance between the moving and stationary plates (Figure 3). An accelerometer was later mounted on the case to determine the relative position of the plates with respect to noise.

All outputs were conditioned to be either displayed on an oscilloscope or recorded on a digital multipoint recorder.



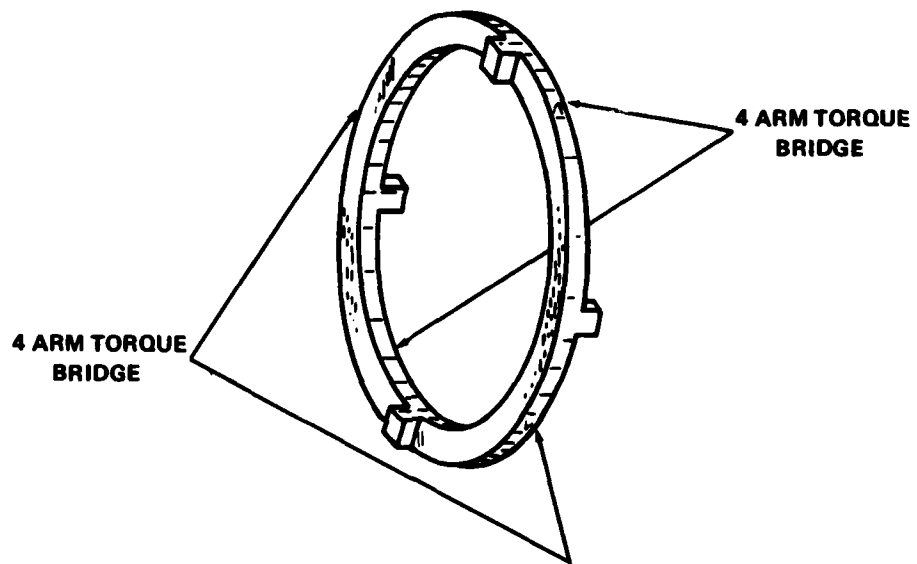


Figure 6 - Position of Strain Gages on Oldham Ring --  
First-Generation Pump

## OPERATION

A series of tests were conducted lasting two to four hours in duration. Before the start of each test, the plates were positioned manually (for gap clearance) and a check was made to ensure that the seal behind the moving plate was seated. Nitrogen was used to supply a positive head of 25 to 40 psi ( $1.7$  to  $2.7 \times 10^5$  Pa) and the oil was circulated through the heat exchangers to maintain a uniform 100 F (38 C) temperature.

Each test consisted of bringing the pump up to a prespecified discharge pressure. Then, by regulating the pressure behind the moving plate, data was collected for various ratios of discharge pressure to pressure behind the plate. Temperatures and pressures (see "Instrumentation" section above for list) were recorded on a data logger which would be used later to determine the operating efficiencies at different conditions. An oscilloscope and camera were used in conjunction with the linear voltage displacement transducer to record the distance between the plates.

## RESULTS--FIRST-GENERATION PUMP

Initially, the pump was operated one hour, disassembled and inspected. The wear patterns on the two scroll plates indicated it was necessary to correct the phase angle between the two plates. This procedure was repeated until the correct phase angle was obtained. The wear pattern still showed that the two plates were hitting on the outside edges of the vanes. The outside radius of the vanes on both plates was reground to eliminate the possibility that the plates were separating because of the interference at these radii. This was repeated until there was no longer evidence that the radii were hitting. Static leakage out of the discharge port was measured with the suction chamber and the area behind the moving scroll plate pressurized to 100 psi ( $6.9 \times 10^5$  Pa). These results are shown in Figure 7 as a function of drive shaft angle. The position of the scroll plates and the shape of the radii were not changed for the remainder of the evaluation.

The force pushing the moving scroll plate into the stationary scroll plate was determined to have a significant effect on the volumetric

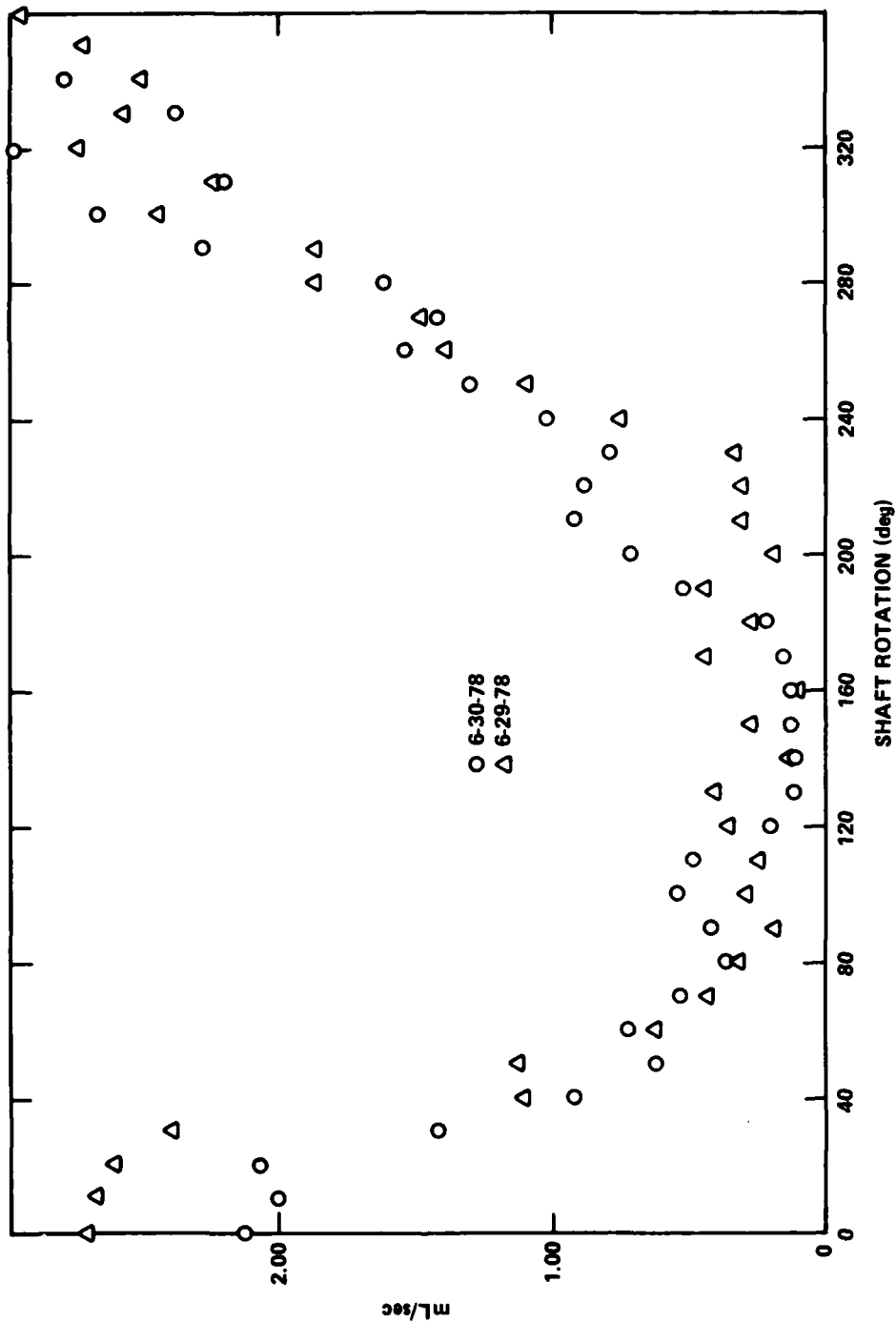


Figure 7 - Static Leakage Test -- First-Generation Pump

efficiency of the pump. Figure 8 shows the effect this force had for constant discharge pressures. The force behind the moving scroll plate was produced by fluid pressure tapped from the discharge line. The abscissa of Figure 8 is the ratio of pressure behind the moving scroll plate divided by pump discharge pressure. This ratio will henceforth be referred to as the closure ratio. Volumetric efficiency versus discharge pressure, at a constant closure ratio equal to 0.75, is shown in Figure 9. Overall efficiency versus discharge pressure is plotted in Figure 10, which shows the values for three days of operation. The points corresponding to a closure ratio of 0.75 are also shown.

The force applied to the Oldham ring was monitored on an oscilloscope. The trace verified calculations that the moment about the center of the moving scroll changes direction every 90 deg of drive shaft rotation. The amplitude of the average torque was very low but, as shown in Figure 11, the change in direction was readily apparent. The upper trace on Figure 11 is an indication of shaft rotation, a signal being registered every 90 deg.

The linear voltage displacement transducer indicated the axial position of the moving scroll plate only up to approximately 500 psi ( $3.4 \times 10^6$  Pa) discharge pressure. Beyond that pressure, the trace from the displacement transducer showed that the moving plate had moved into the stationary plate which is not possible.

Evaluation of the pump was stopped when the volumetric efficiency dropped off suddenly. The unit was disassembled and inspection revealed that the two scroll plates had galled between a vane tip and the opposing valley. Figure 12 is a view of the damaged area on the moving plate and Figure 13 shows the stationary plate.

#### DISCUSSION--FIRST-GENERATION PUMP

The mathematical model of leakage past the scroll's vane flanks is described in Appendix B. Another leakage path in the scroll pump is across the tip of the vanes. This can be modeled by employing equations presented by Stepanoff.<sup>2</sup> In Stepanoff's case, the leakage path is a diametral clearance; whereas the leakage path in the scroll can be

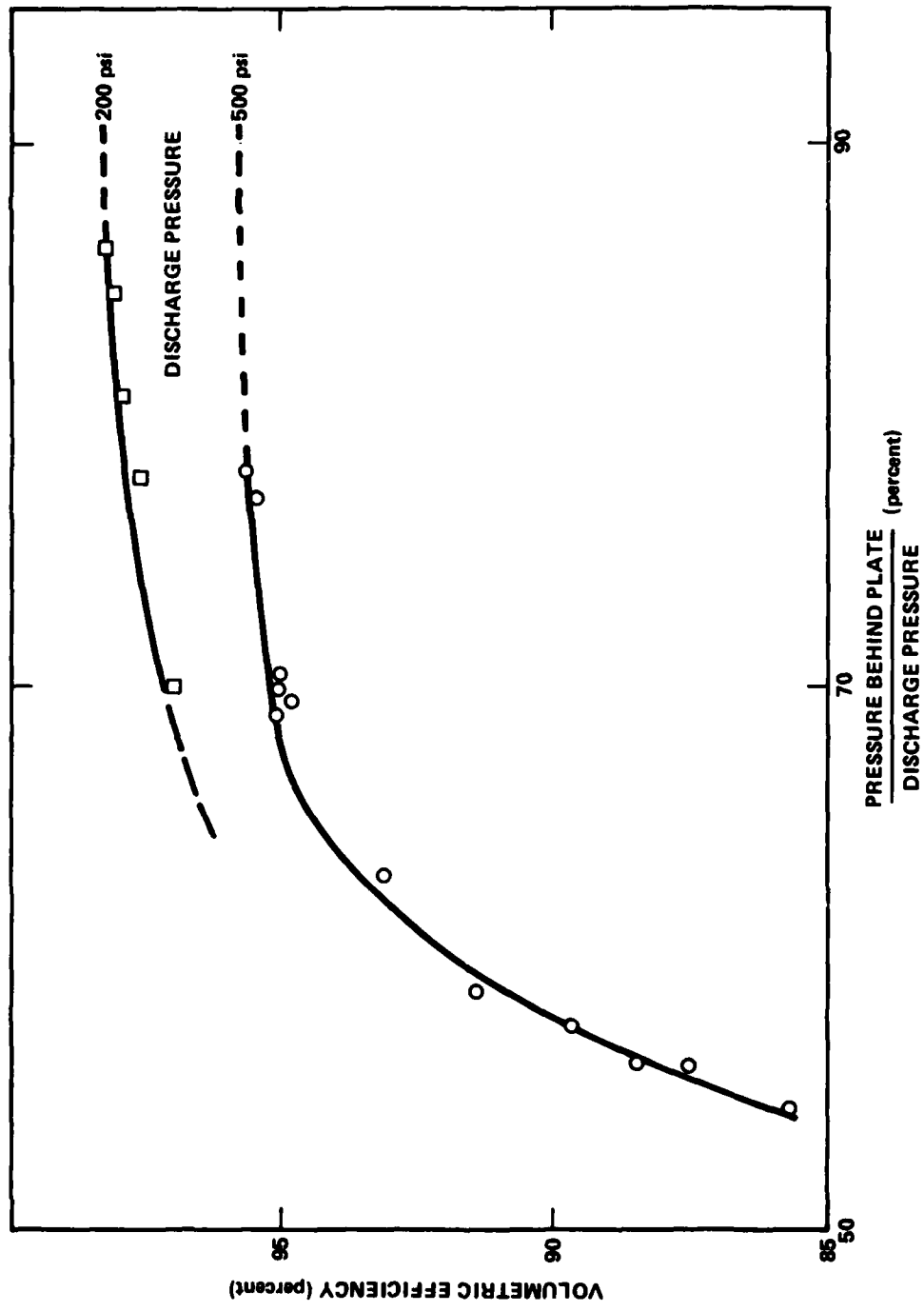


Figure 8 - Effect of Pressure Behind Moving Scroll Plate on Volumetric Efficiency -- First-Generation Pump

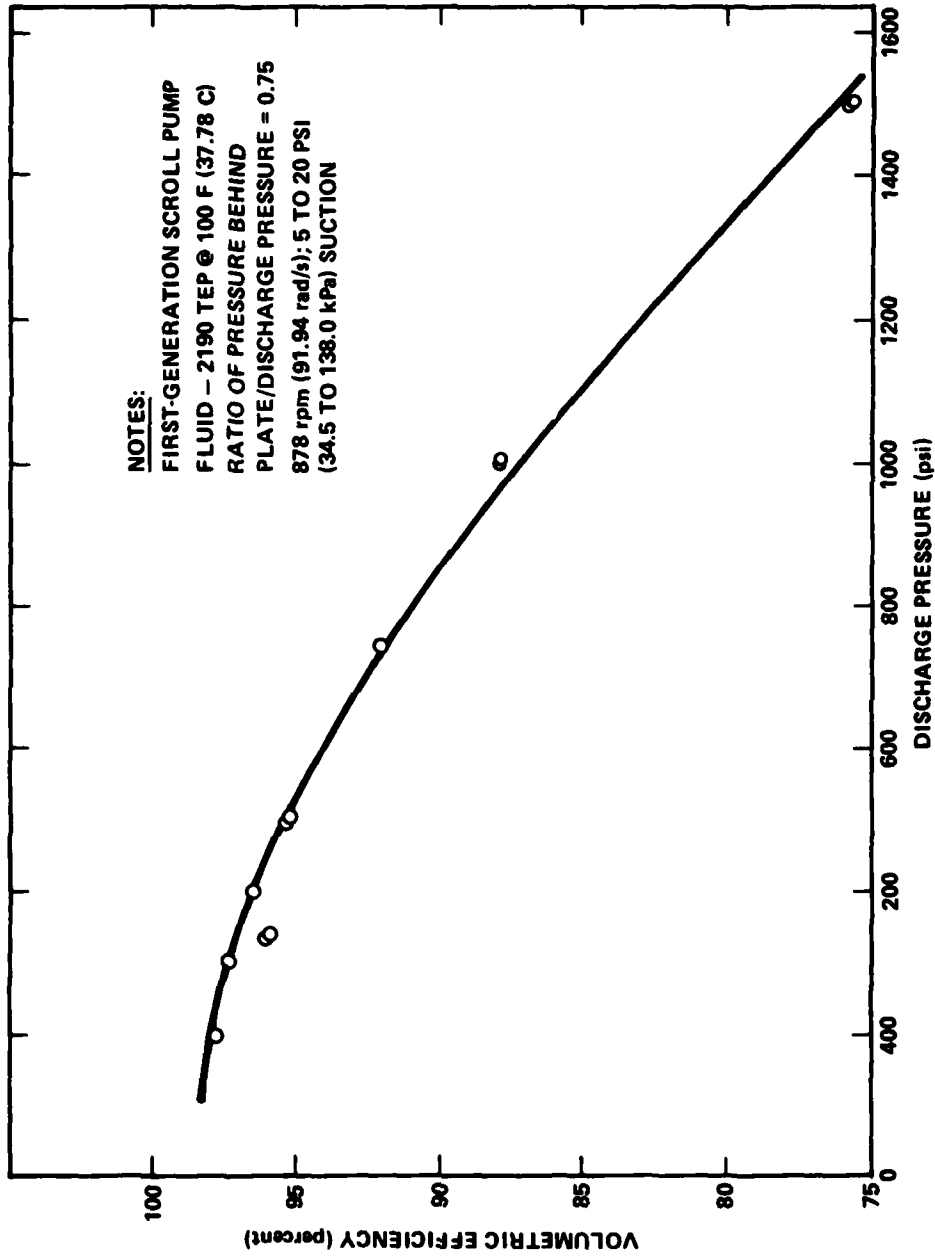


Figure 9 - Volumetric Efficiency -- First-Generation Pump

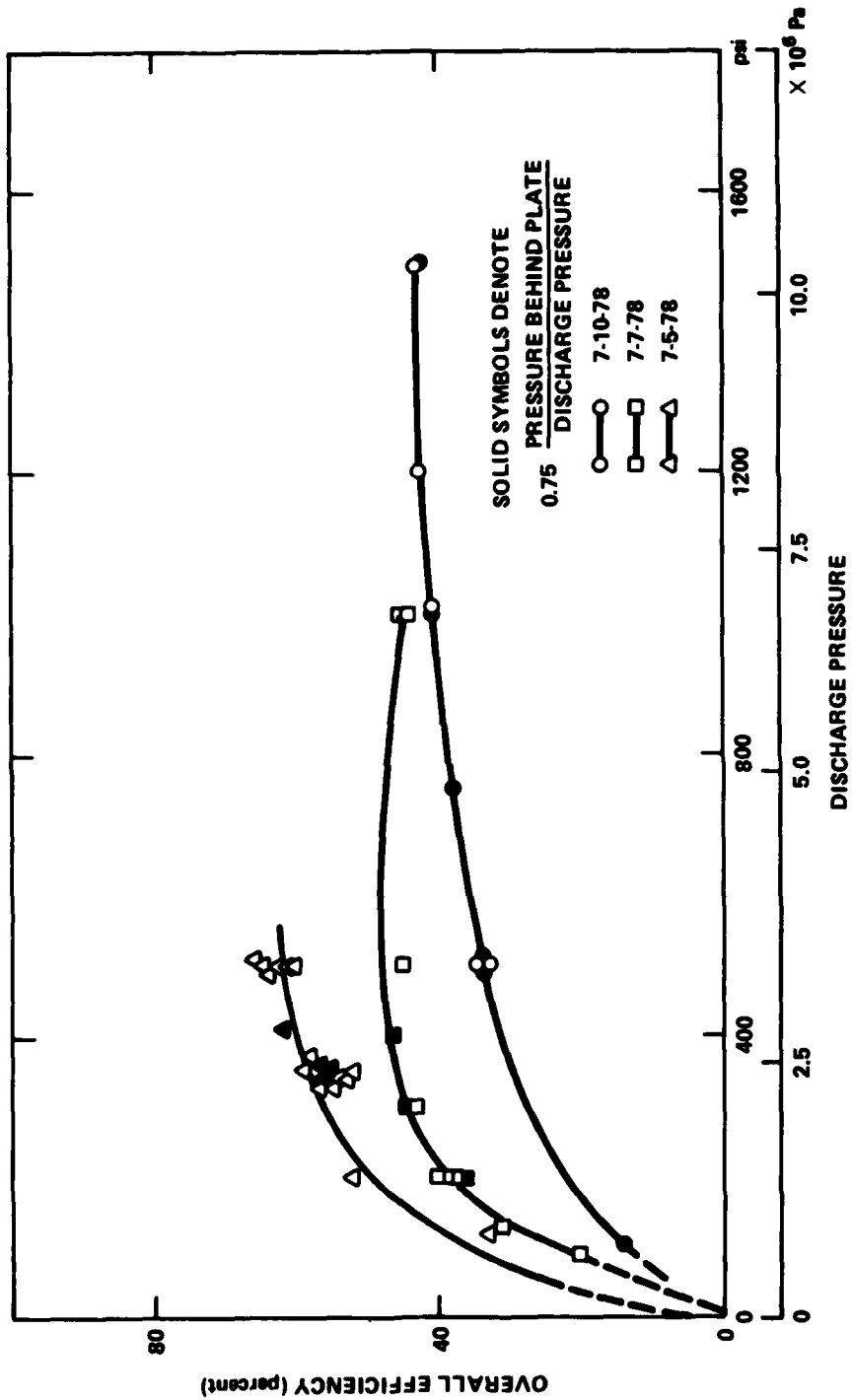


Figure 10 - Overall Efficiency -- First-Generation Pump

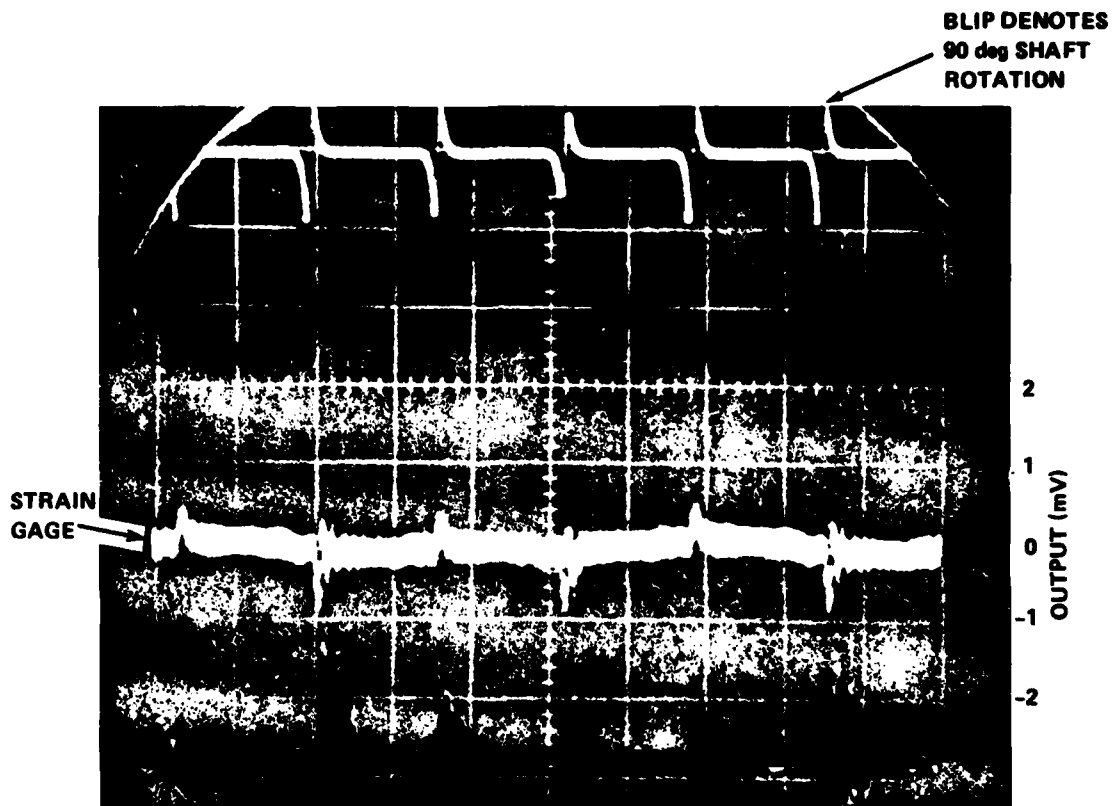


Figure 11 - Torque Applied to Oldham Ring -- First-Generation Pump





Figure 12 - Damaged Moving Scroll Plate -- First-Generation Pump



Figure 13 - Damaged Stationary Scroll Plate --- First-Generation Pump

visualized as a diametral clearance which has been straightened out. These equations should yield a good approximation of the leakage flow rate.

With this assumption, predictions of volumetric efficiency were made based on the geometry and running conditions of the first-generation pump. Figure 14 shows the volumetric efficiency predictions plotted for various flank clearances with the tip clearance equal to zero. Figure 15 shows the predicted volumetric efficiency plotted for various tip clearances with the flank clearance equal to zero. From a comparison of the two graphs, it is apparent that tip clearance has a greater influence on volumetric efficiency than does the flank clearance. This is as expected because the tip leakage path is much shorter than the flank leakage path.

When the static leakage test was conducted (Figure 7), the area behind the moving scroll plate was pressurized and the discharge port was open to atmosphere. If it is assumed that the tip clearance is zero in this condition, the flank leakage model can be applied by using average values of the observed static leakage and the pressure difference to determine a flank clearance. This clearance was calculated to be 0.0025 in. (63.5  $\mu\text{m}$ ). The leakage due to the above calculated flank clearance was then added to the leakage of various tip clearances for the same pressure. To aid in a comparison of predicted versus observed data, the calculated leakage is shown in Figure 16 along with the volumetric efficiency measured with a closure ratio equal to 0.75. The line for a tip clearance equal to 0.002 in. (50.8  $\mu\text{m}$ ) is in good agreement for pressures less than 500 psi ( $3.4 \times 10^6$  Pa). The flank clearance cannot change because it is mechanically constrained; but the tip clearance can change because the moving plate is not positively located in the axial direction. Therefore, it appears that above 500 psi ( $3.4 \times 10^6$  Pa) the tip clearance increased.

This corresponds to the point where the linear transducer was no longer able to track the axial position of the moving plate. To better understand this, the forces on the moving scroll in the axial direction were examined. From this examination, it was determined that when the volume in a pocket changes from suction to discharge it does so very fast,

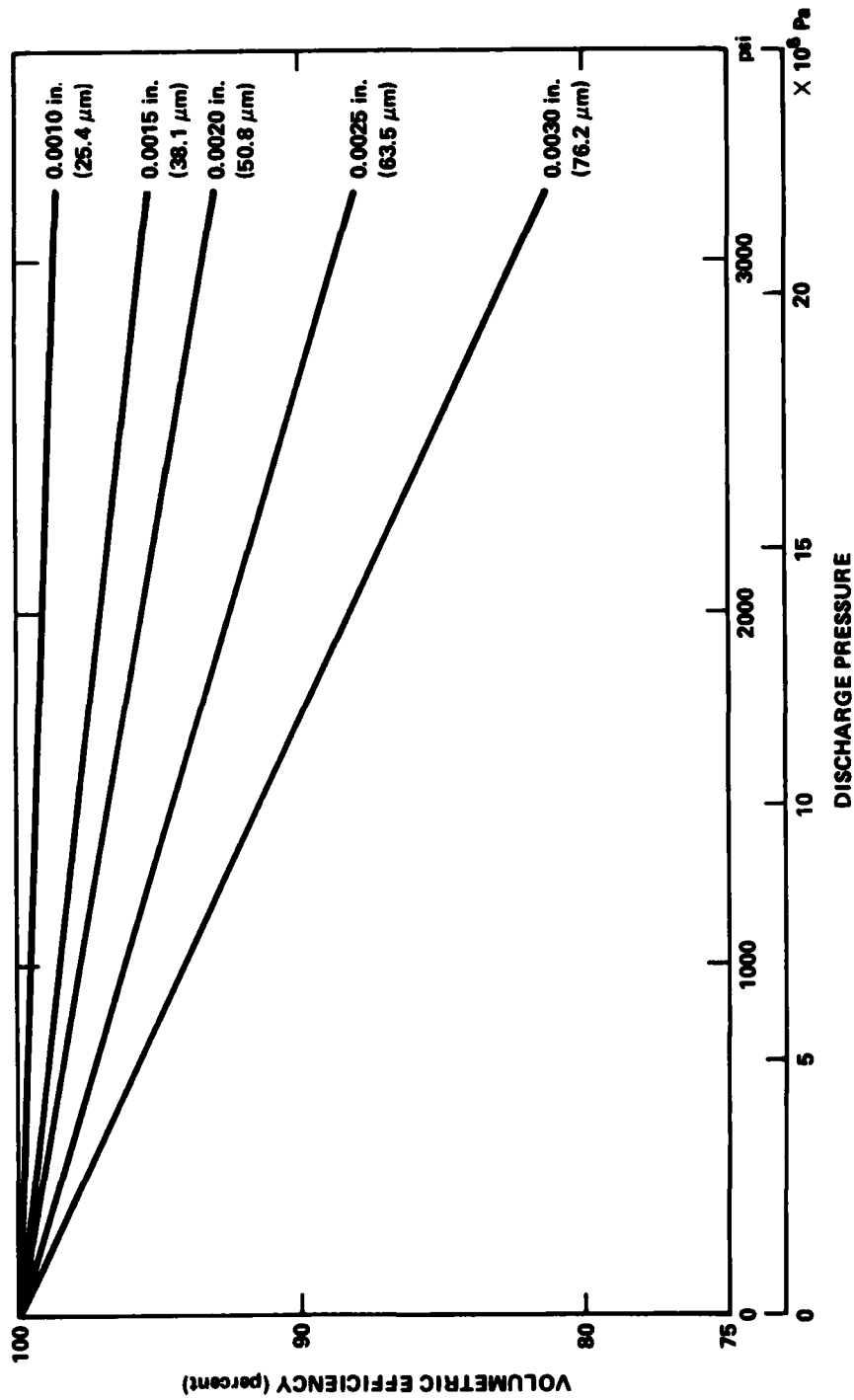


Figure 14 - Predicted Volumetric Efficiency for Various Flank Clearances with Tip Clearance = 0.0 in. -- First-Generation Pump

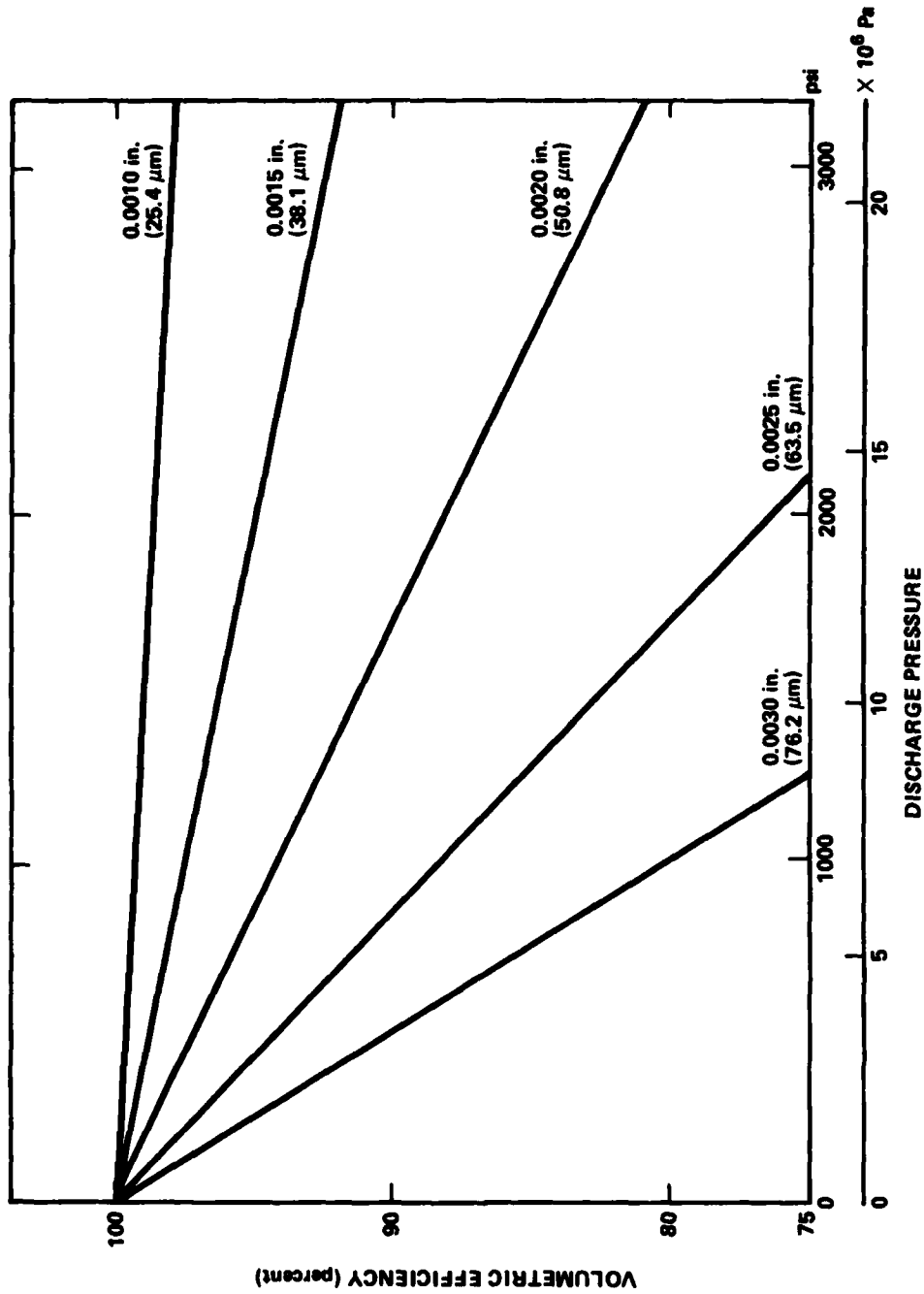


Figure 15 - Predicted Volumetric Efficiency for Various Tip Clearances with Flank Clearance = 0.0 in. -- First-Generation Pump

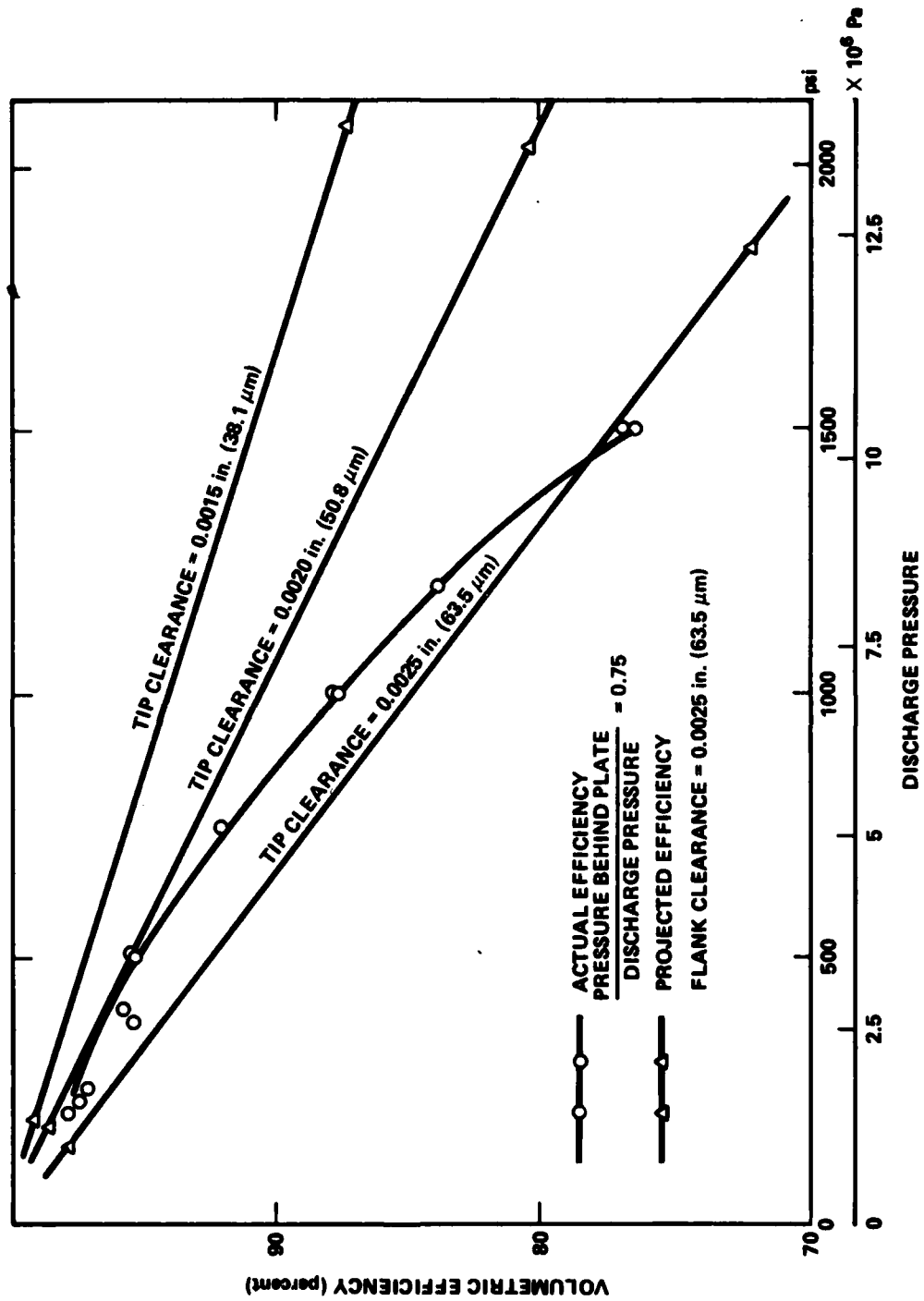


Figure 16 - Comparison of Actual and Projected Volumetric Efficiencies

resulting in a large change in the force pushing the scroll plates apart. This was modeled using the following assumptions: (1) the pressure profile across a scroll vane is linear when there is discharge pressure on one side and suction pressure on the other; (2) the maximum force trying to open the scroll plates occurs when the pocket is at discharge pressure; (3) the minimum force trying to open the scroll plates occurs when the pocket is at suction pressure; and (4) the force trying to open the scroll at other points in the cycle is a linear relationship between the maximum and minimum. This prediction is shown in Figure 17. The force trying to close the scroll plates is produced by the pressure applied behind the moving scroll plate. This is a constant force and would be a horizontal line on the figure. The closing force can be adjusted so that it is sufficient to keep the scroll plates together when the opening force is a maximum. However, when the opening force is at a minimum the closing force would then be pushing the scroll plates together with a force equal to the difference between the maximum and minimum opening forces.

When the required closure ratio was calculated using the model, the result was a closure ratio of 0.45 to 0.50 for the full pressure range. This is much less than the closure ratio necessary to get the maximum volumetric efficiency (Figure 8) in the operating pump. The explanation would be that the pressures in the discharge area and behind the moving scroll plate are not fully understood. However, it is certain that the axial force fluctuates an amount at least equal to the pocket area normal to the scroll plate multiplied by the discharge pressure.

The need to enlarge the external radius on the sides of the scroll vanes showed that the lapping procedure produced good results on the flat surfaces; but it did not produce a uniform shape in the corners. The need to enlarge the external radius on the flat tips of the scroll vanes shows that the phase angle (Appendix A) between the scroll plates was not held as precisely in the pump as it was in the lapping fixture. The phase angle was held by the Oldham ring in both the pump and the lapping fixture and the clearances were the same. The difference was that the Oldham ring in the pump was positioning the phase angle on a smaller

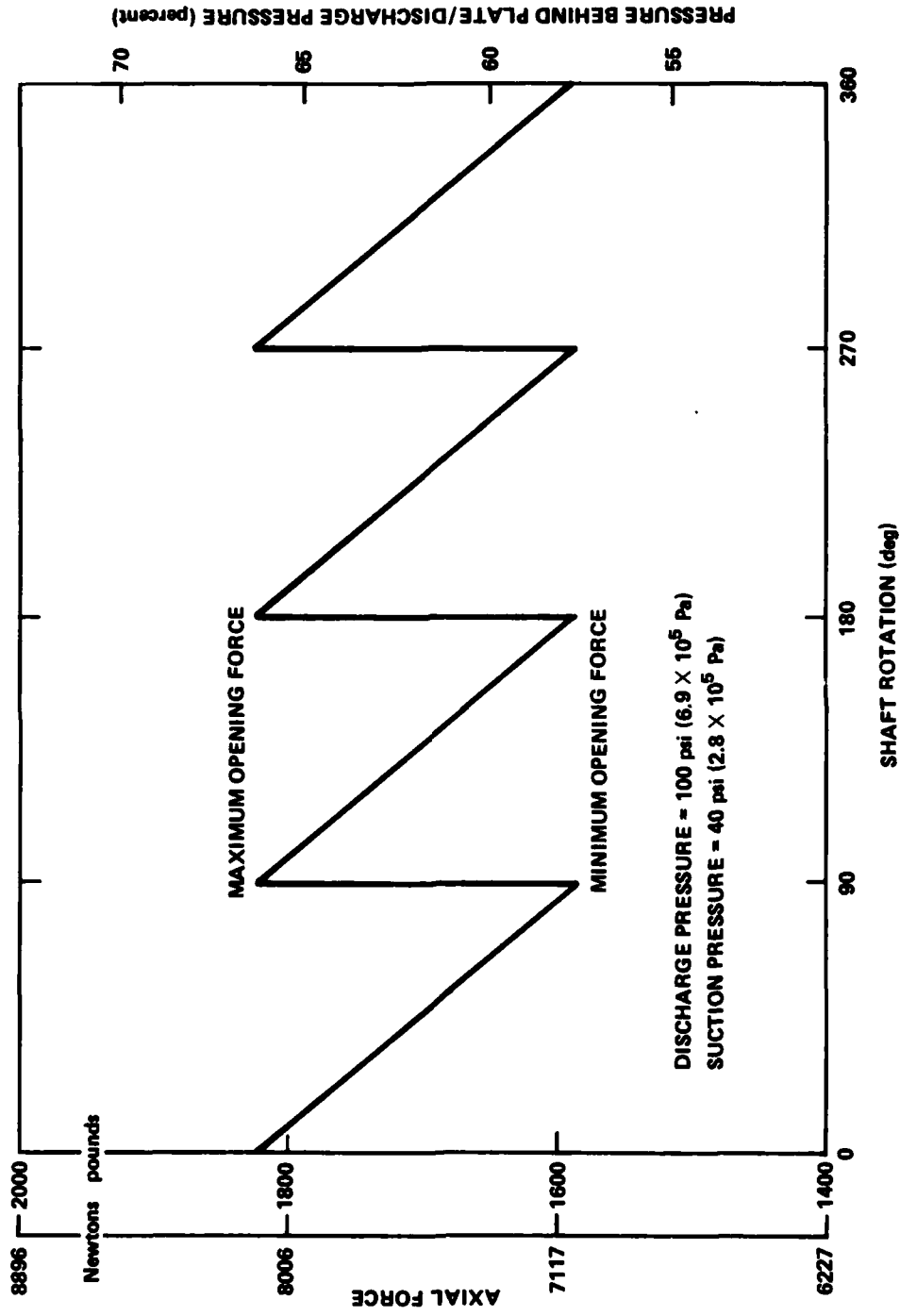


Figure 17 - Axial Forces on the Moving Scroll Plate -- First-Generation Pump



diameter than in the lapping fixture. So for the same clearances the phase angle change was greater in the pump.

The overall efficiencies (Figure 10) showed widespread differences from run to run. The overall efficiency was expected to be low at lower pressures because the losses would be a higher percent of energy input. There is no apparent explanation.

## DESCRIPTION OF PROTOTYPE--SECOND-GENERATION PUMP

### BASIC DESIGN

The second-generation pump uses a synchronously rotating drive method to generate the required relative motion between the two scroll plates.<sup>3</sup> Figure 18 is a sectional view of the pump. Briefly described, the drive is accomplished by directly mounting the driver scroll plate on the centerline of the input drive shaft. The driven scroll plate is mounted about its own center on bearings so that the centerlines of the scroll plates are parallel, but not colinear. An Oldham ring is mounted between the two plates to maintain proper phase angle, but to allow for the different centerline positions. With this arrangement, both scroll plates rotate synchronously about their own center so balancing is straightforward. The Oldham ring rotates, but it also orbits twice for each shaft revolution on a diameter equal to the orbiting radius between the scroll plates. The Oldham ring is not balanced; however, the unbalanced force is not significant.

Pumping is accomplished in a manner similar to that described for the first-generation pump. The pump suction chamber is at the center of the two scroll plates. The discharge chamber is around the outside diameter of the two plates. Figure 19 shows the progression of the pocket when both plates rotate. The driven scroll plate is mounted so that the orbiting radius can be adjusted. There are two mechanical face seals behind each of the scroll plates. In operation, the pressures in the areas between the seals were controlled to provide for axial positioning of the two scroll plates. A low-pressure mechanical shaft seal is used where the drive shaft passes through the case. The capability to

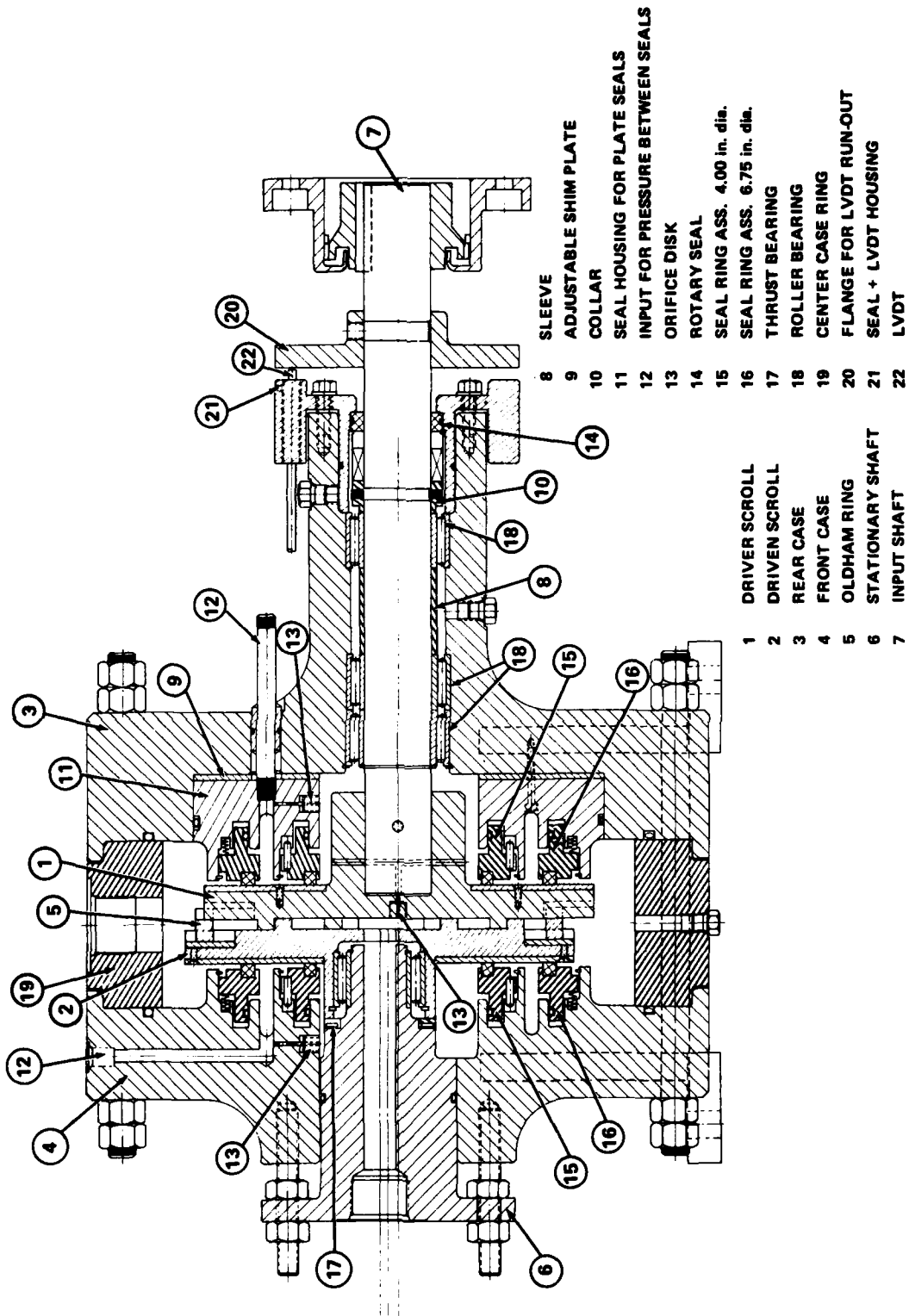


Figure 18 - Cutaway of Second-Generation Pump

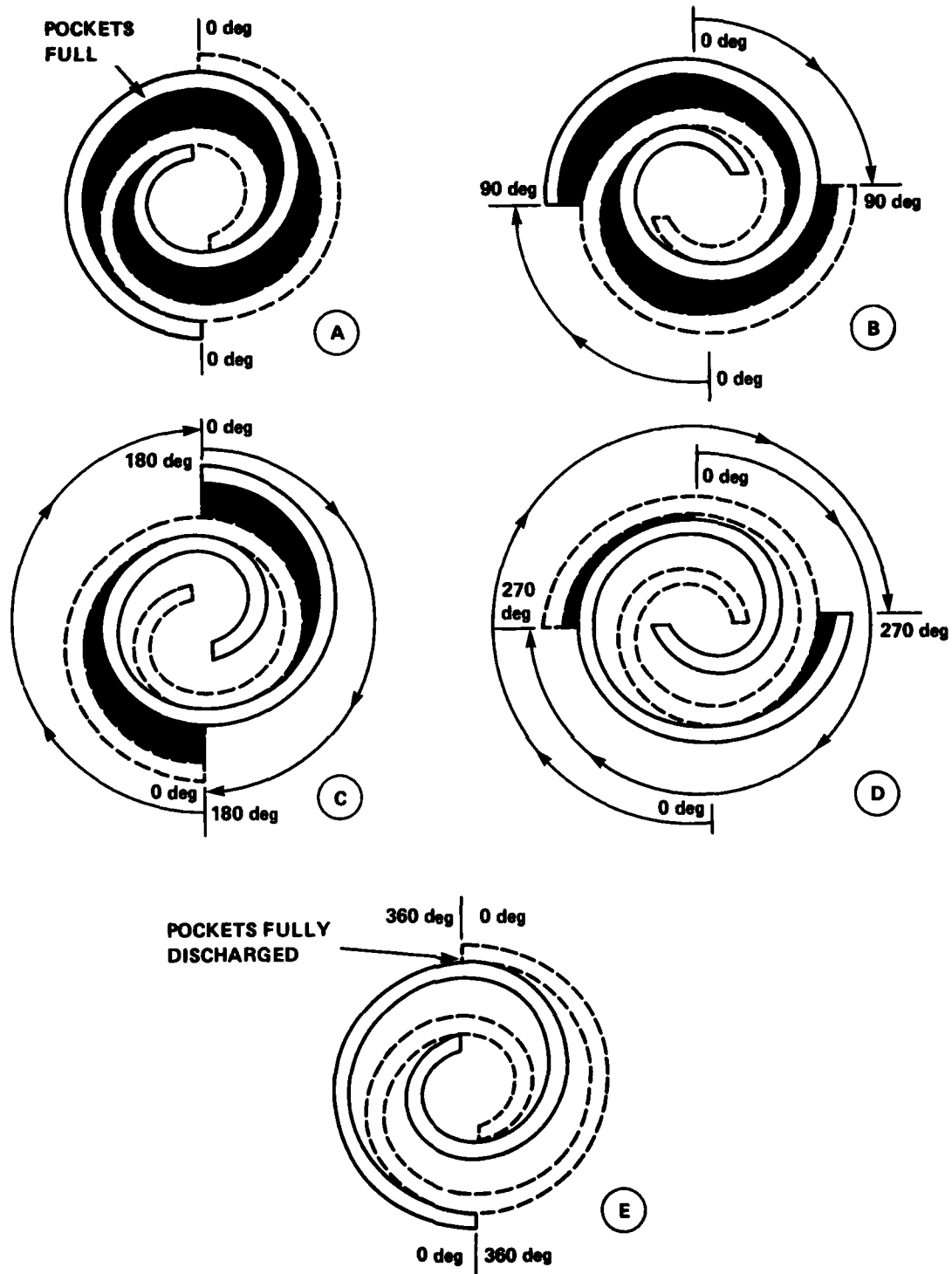


Figure 19 - Pocket Progression -- Synchronously Rotating Drive -- Second-Generation Pump

dynamically balance the synchronously rotating scroll plates made it advantageous to increase the orbiting radius because the radial bearing load can be approximated by dividing the input torque by the orbiting radius. Therefore, for a given input power, the larger the orbiting radius, the lower the radial bearing load.

The rate of change of the volume of the pocket between two scroll vanes at the time when discharge begins is less when pumping from inside to outside than the converse. The volume in a pocket for pumping in both directions is shown in Figure 20. Because the rate of change of the volume is less, the overpressurization of a pocket in the second-generation pump is reduced. The overpressurization was considered negligible, and it was decided to evaluate the pump first without the additional discharge ports used in the first-generation pump.

#### FABRICATION

Conventional machining techniques were used for all of the components except the scroll plates. These were machined with a vertical milling machine equipped with a traversing table geared to a horizontally mounted rotary table. After machining, the plates were lapped in a fixture similar to that described for the first-generation pump. After the proper phase angle was located and the lapping was finished, the Oldham ring inserts and the Oldham ring were fitted to produce the required phase angle between the two scroll plates. Then, the plates were removed from the fixture and balanced separately. Figure 21 shows the driver scroll plate and the Oldham ring guides after balancing.

#### TEST PROCEDURE--SECOND-GENERATION PUMP

##### SYSTEM DESCRIPTION

The second-generation pump's piping system is basically the same as that for the first-generation pump.

The only modification to the piping system is control of the pressure in the areas behind both plates. Tubing was installed to control the pressure in the seal cavity behind the driver plate. With this

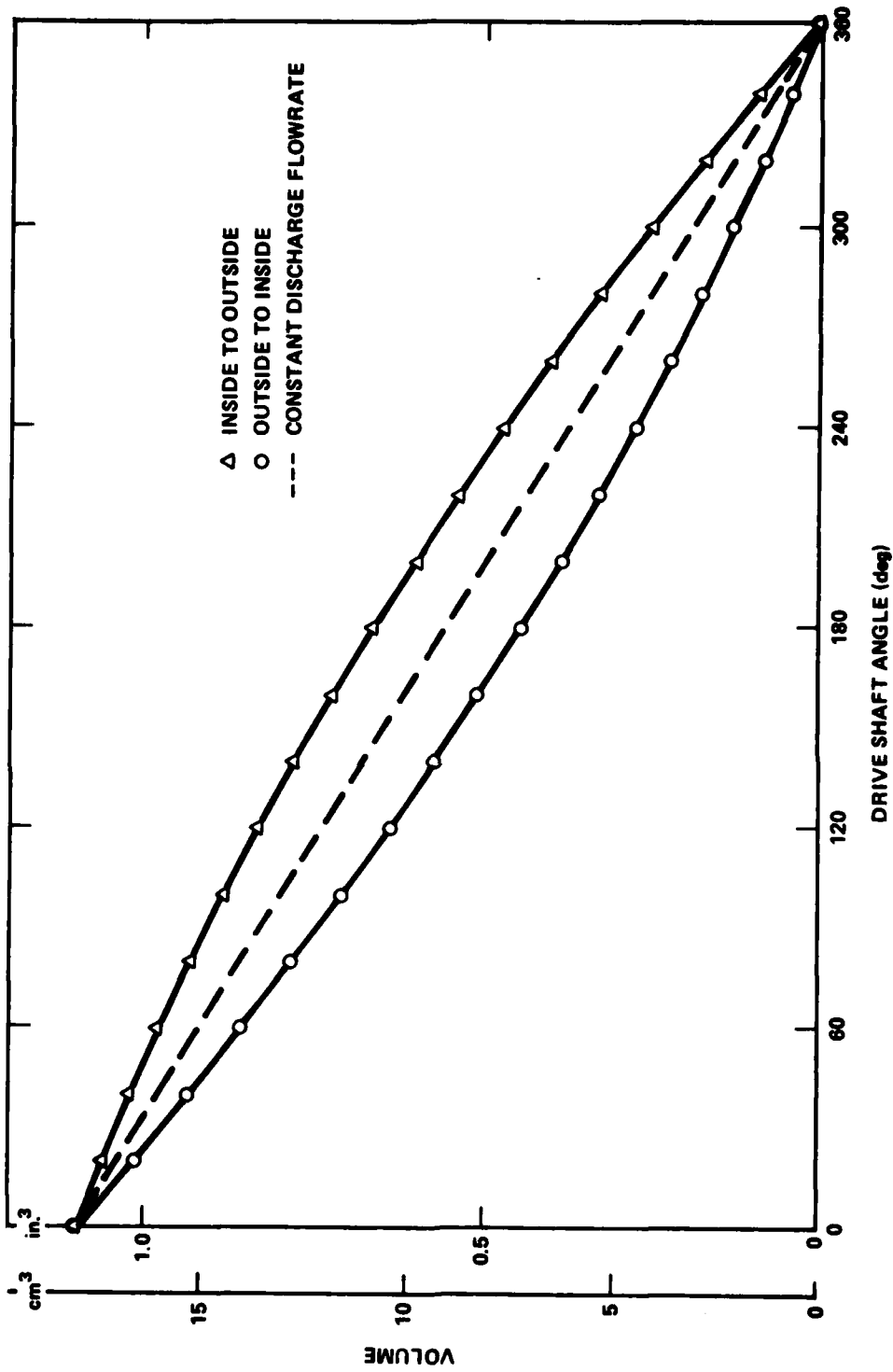


Figure 20 - Pocket Volume Progression -- Synchronously Rotating Drive --  
Second-Generation Pump

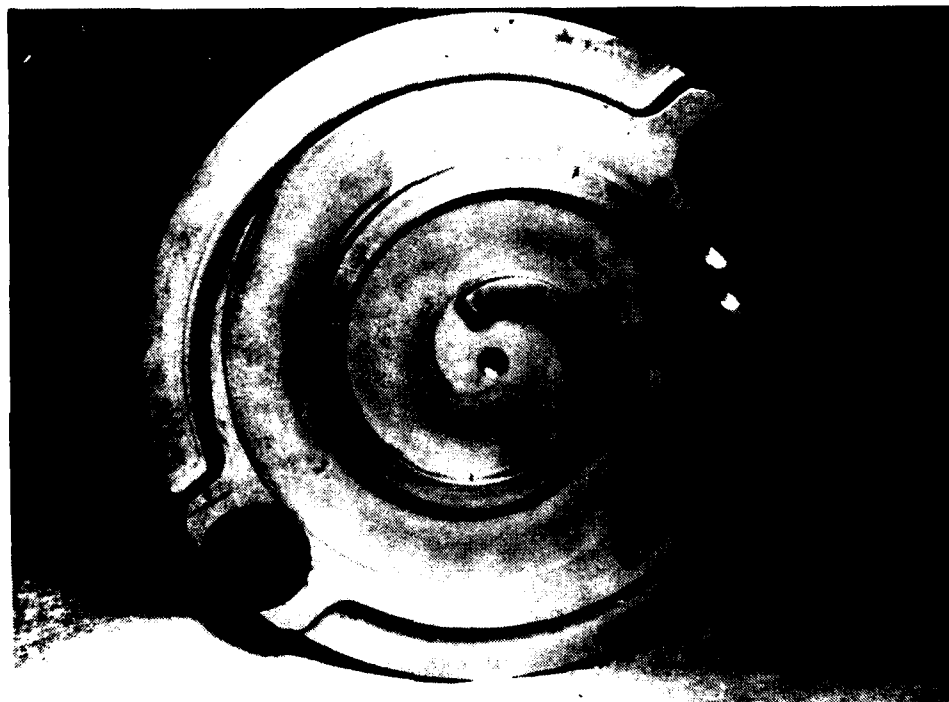


Figure 21 - Driver Scroll Plate -- Second-Generation Pump

arrangement, the force necessary to keep the two rotating scroll plates together is applied behind both plates at the same time.

The pump is driven by a direct-coupled 30 hp (22.4 kW) variable speed dc motor.

#### INSTRUMENTATION

Instrumentation and parameters measured on the second-generation pump remained the same as those for the first-generation pump.

The linear voltage-displacement transducer could be mounted externally to measure the distance the shaft moved axially, because the input shaft was directly connected to the driver scroll. The transducer was mounted so that it measured the movement of a disk attached to the input shaft (Figure 18).

#### OPERATION

As in the first-generation pump, a test run was four hours or less in duration. As explained in the system description, the two plates were located axially by pressure control. Nitrogen supplied a positive head of 25 to 40 psi ( $1.7$  to  $2.7 \times 10^5$  Pa) and the oil was maintained at a uniform temperature of 100 F (38 C).

The dc motor was started at its lowest speed (approximately 200 rpm). Then, the cavities behind the plates were pressurized to bring the plates together. Discharge pressure was controlled either by throttling the discharge or by varying the speed of the motor. Discharge pressure could also be controlled to a small degree by the axial location of the plates.

Data was taken for a constant discharge pressure at various motor speeds and plate clearances. The data was then reduced and analyzed. If conditions warranted, the pump was disassembled and inspected. After reassembly, a new test was run at a different discharge pressure.

#### RESULTS--SECOND-GENERATION PUMP

The pump was operated at discharge pressures of less than 200 psi ( $1.4 \times 10^6$  Pa) and at various speeds to evaluate the drive arrangement.

The drive operated quietly and smoothly through a speed range of 200 to 2800 rpm in spite of unbalanced Oldham ring forces computed to be 41 lbf (182.4 N) at 2800 rpm.

When compared to the first-generation pump, control of the phase angle between the two scroll plates was improved in the second-generation pump for two reasons. First, the diameter of the Oldham ring in the second-generation pump was larger than the one used in the first-generation pump; so for the same clearances, the angle change in the second-generation pump would be less. Second, the Oldham ring used in the second-generation pump was fitted between the two scroll plates while the plates were still in the lapping fixture; whereas the Oldham ring used in the first-generation pump was aligned in the pump housing. This produced an initial misalignment of the phase angle in the first-generation pump that was corrected before the evaluation of the performance of the pump began. The improved control of the phase angle was verified when the scroll plates in the second-generation pump were inspected after operation. The external radius of the scroll vanes did not show a heavy wear pattern. The wear pattern on the flat portions of the vanes was also very uniform, which again indicates a more correct phase angle.

When the scroll plates were pushed into each other by pressurizing the areas behind the plates the flowrate increased as would be expected. But, as more pressure was applied, violent pressure surges began. Modifications were made to the piping network to reduce the variations in the force pushing the plates together, but no improvement resulted. The source of supply for the pressure behind the plates was changed from the discharge line to a pulsation-free source. The violent pressure surges could not be eliminated.

The closure ratio (i.e., pressure behind the plates divided by the discharge pressure) versus shaft speed is shown in Figure 22. The volumetric efficiency versus shaft speed is shown in Figure 23. The data for both of these figures were taken when the pressure surges first began.

While obtaining these data, the guides that positioned the Oldham ring failed. However, neither the scroll plates nor the vanes were damaged. Figures 24 and 25 show the Oldham ring and the Oldham ring guides.



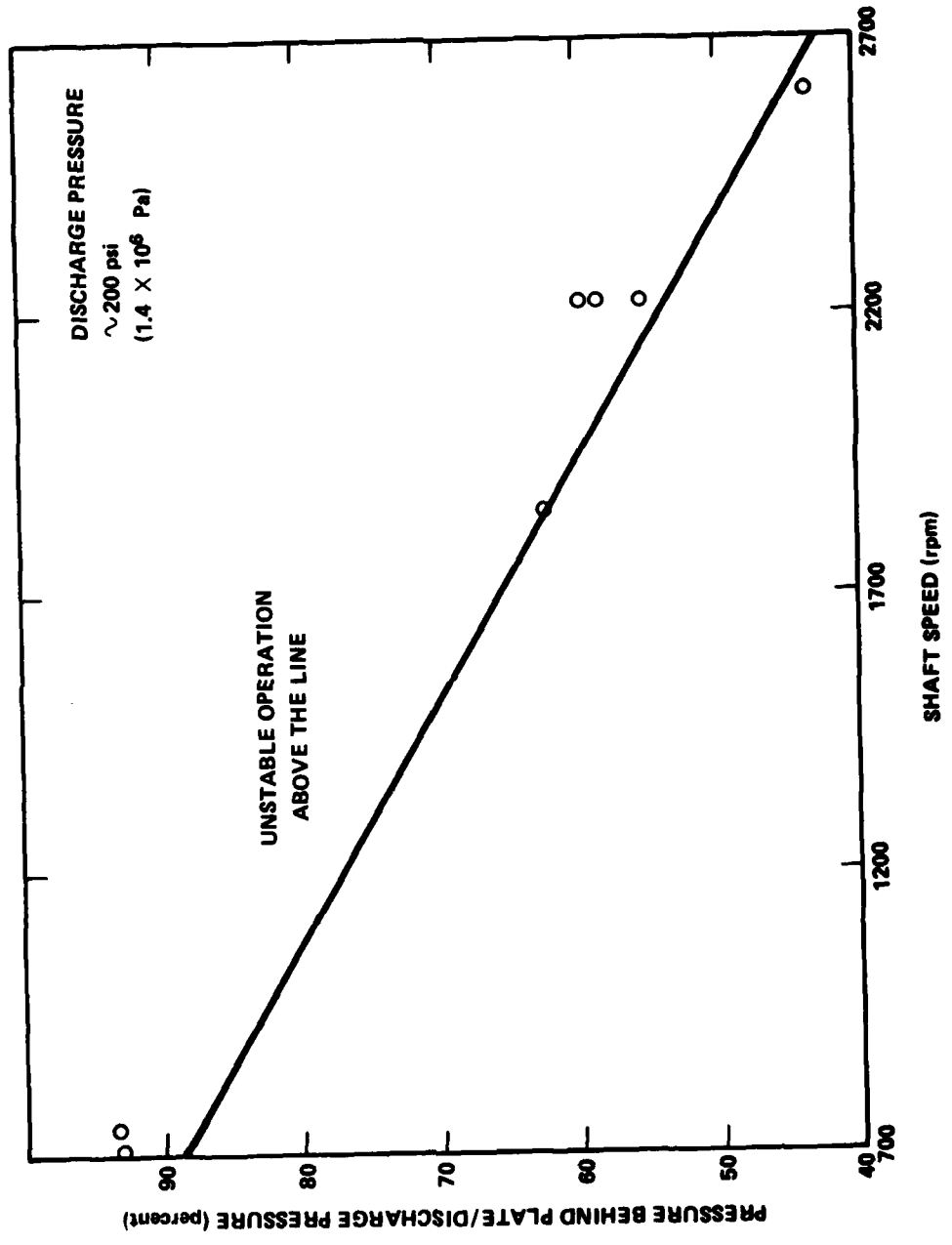


Figure 22 - Occurrence of Large Pressure Fluctuations -- Second-Generation Pump

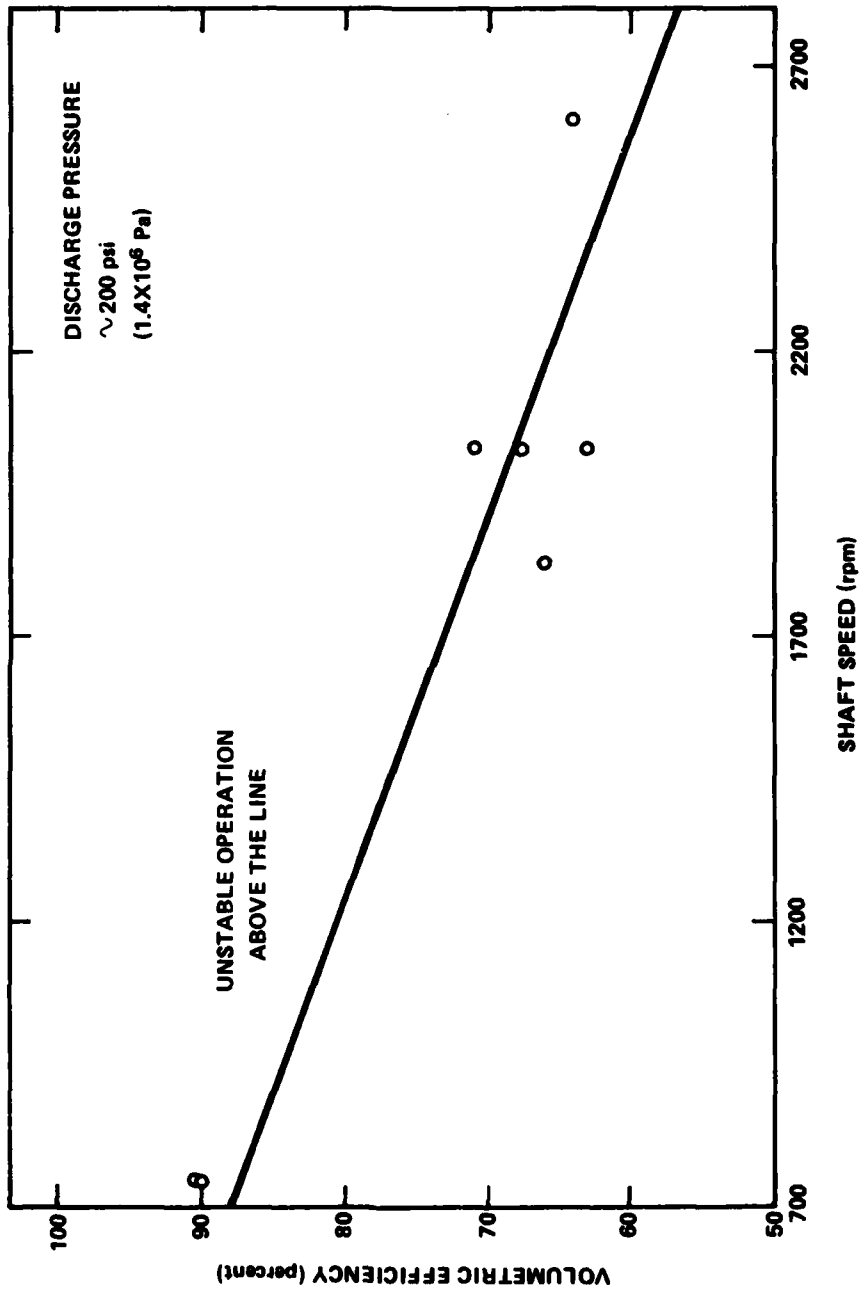


Figure 23 - Volumetric Efficiency at Points Where Pressure Fluctuations Occurred -- Second-Generation Pump

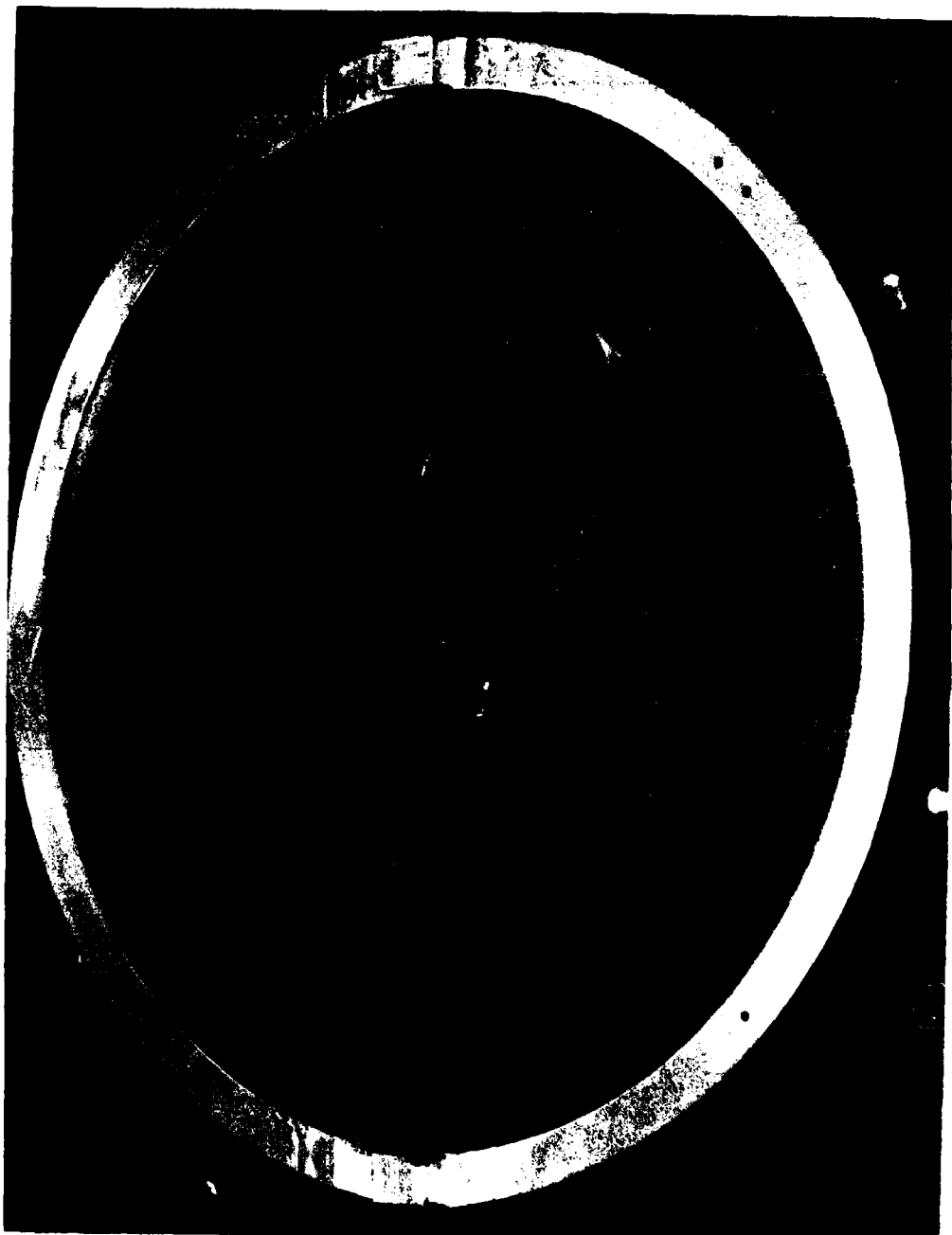


Figure 24 - Damaged Oldham Ring -- Second-Generation Pump

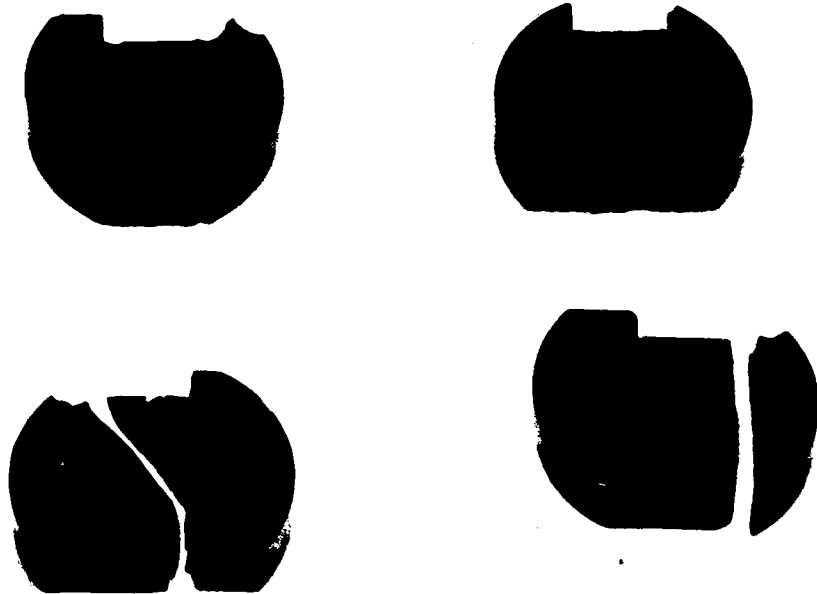


Figure 25 - Damaged Oldham Ring Guides -- Second-Generation Pump

#### DISCUSSION--SECOND-GENERATION PUMP

The pressure surges were caused by fluctuations in the axial forces (which control their relative position) on the scroll plates. These are the same abrupt force changes as those discussed with regard to the first-generation pump, but the magnitude is much greater for the same discharge pressure (Figure 26). This is a consequence of using a larger orbiting radius to reduce the radial bearing loads in the original design. The scroll plates form two pockets, but they both discharge at the same time; hence, the area normal to the scroll plate that discharges at the same time is larger. The result is that the full, displaced volume of the pump changes from suction pressure to discharge pressure at the same time. However, the relationship of speed and pressure behind the plates and the point where the pressure surges begin does suggest an explanation of the surges. If the pressure changes in the pockets due to discharge and suction pressure were the same at all speeds, the average force opening the scroll plates would be a constant. In this case, it would be expected that for the same conditions the plates would separate less at higher speeds because the time period required to accelerate the plates away from each other is dependent on shaft speed. However, the pressure surges did not reduce as the shaft speed increased. Therefore, it can be assumed that the force opening the plates increased as the shaft speed was increased. The pressure rise caused by insufficient discharge-port area increases as the shaft speed increases. Therefore, it appears that the forces that moved the plates apart were caused by overpressurization associated with the undersized discharge port area.

Time did not permit installation of additional discharge ports like those used in the first-generation pump. But, the first-generation pump results showed a loss of control of the axial position of the moving scroll plate above 500 psi ( $3.4 \times 10^6$  Pa). If this loss of control of the axial position of the moving scroll plate was also caused by overpressurization associated with insufficient discharge area, then the model used to predict the required discharge area is not correct.

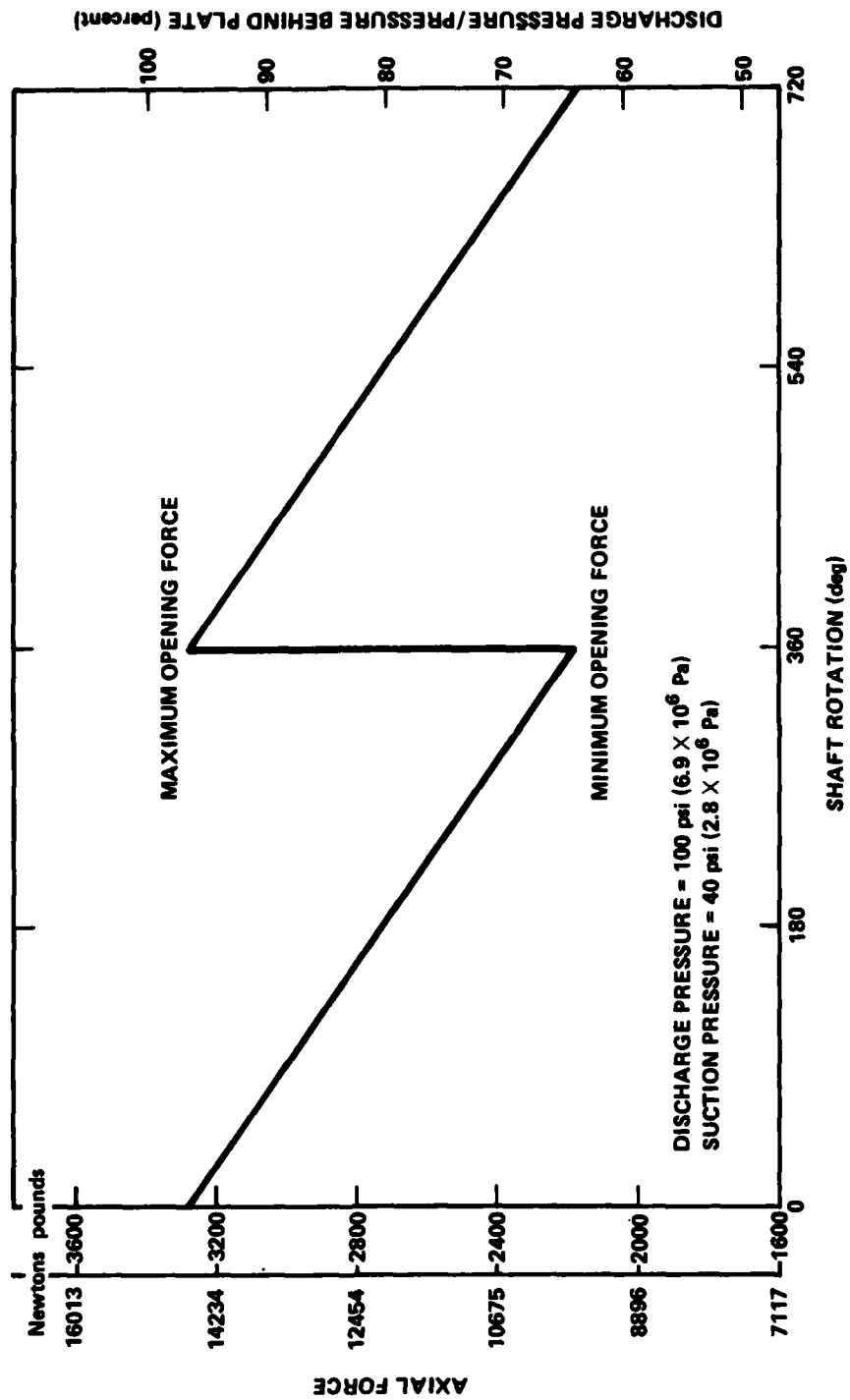


Figure 26 - Axial Forces on the Driver Scroll Plate -- Second-Generation Pump

## CONCLUSIONS AND RECOMMENDATIONS

The first-generation pump demonstrated high volumetric efficiencies at pressures below 500 psi ( $3.4 \times 10^6$  Pa). The leakage model previously discussed was used to plot the predicted volumetric efficiency for combinations of flank clearances and tip clearance in the first-generation pump. This was calculated for a discharge pressure of 3000 psi ( $2.07 \times 10^7$  Pa) and is shown in Figure 27. Figure 27 points out the clearances that must be maintained for a desired volumetric efficiency. The clearances are very small, but they are not out of current machining capabilities.

The second-generation pump with the synchronously rotating drive system allowed higher shaft speeds without the vibration associated with the orbiting drive arrangement. This pump also showed that the mechanism to locate the phase angle should be placed on as large a diameter as possible.

The feasibility of the scroll pump has been established. Further development effort will be necessary to verify the models that have been made and to demonstrate the actual volumetric efficiency. Evaluation of the mechanical efficiency and long-term life is also required.

In view of other pump concepts that are now being developed for naval use, it has been decided not to continue the development of the scroll hydraulic pump at this time. However, if, in the future, other concepts cannot produce their currently projected efficiencies, the scroll hydraulic pump should be reevaluated for continued development.

Future work should take into account the following design recommendations.

### SCROLL PLATES

The scroll plates should be designed with regard to the axial force fluctuations resulting from the change in pressure of the trapped pocket. At the least, a four-pocket geometry should be employed to help minimize this fluctuating force. However, increasing the number of pockets results in a small orbiting radius which can produce prohibitive radial bearing loads that may limit pump life. Therefore, a tradeoff has to be made

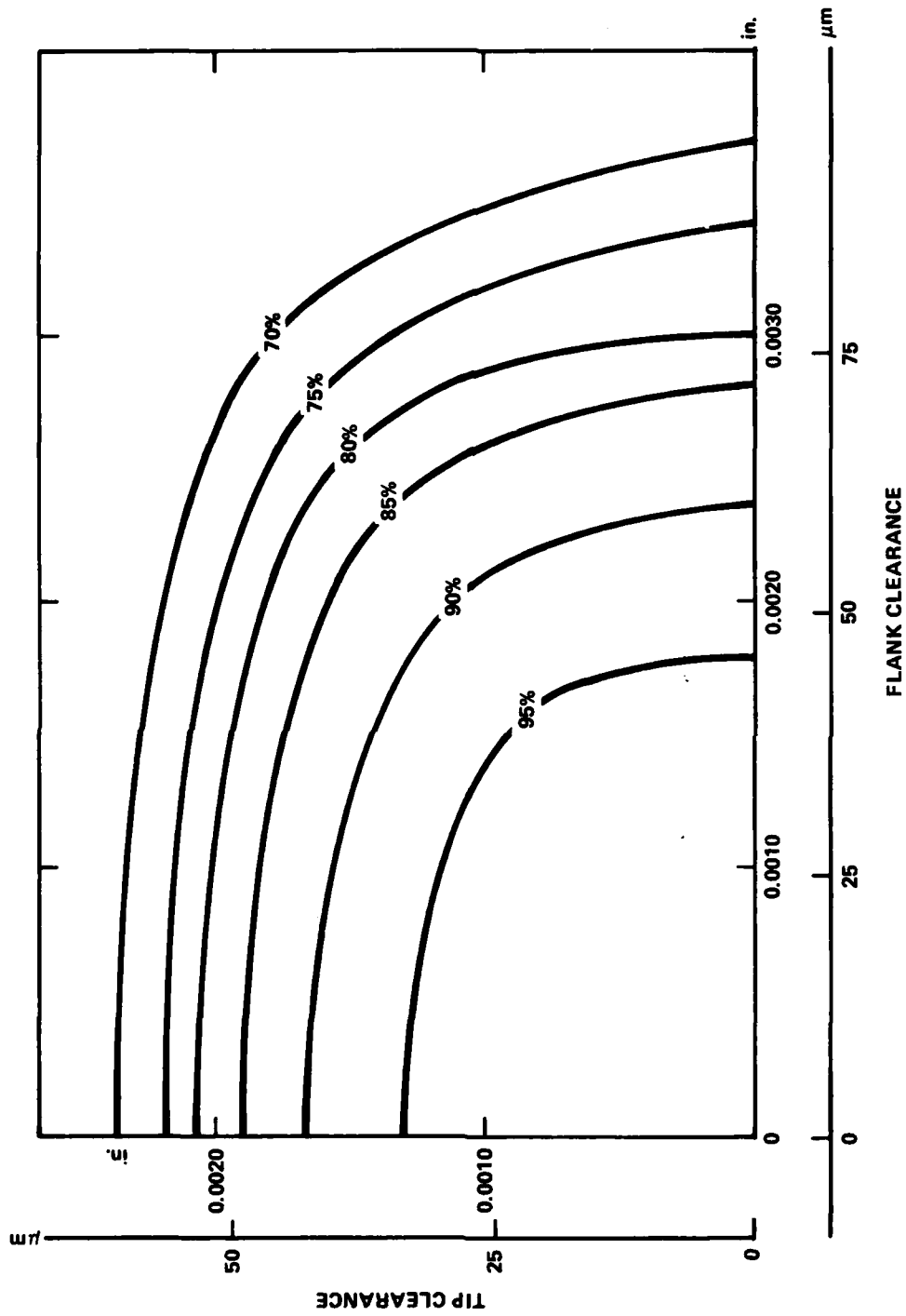


Figure 27 - Predicted Volumetric Efficiencies at 3000 psi ( $2.07 \times 10^7$  Pa) Discharge -- First-Generation Pump



between axial force fluctuations and radial bearing load. The additional discharge ports should be evaluated experimentally to verify the model.

#### DRIVE METHOD

The synchronously rotating drive method, like that used in the second-generation pump, should be used with some modifications. The Oldham ring could be replaced by connecting the two plates via gears on a separate shaft. The pump could also be driven through this extra shaft. The scroll plates would spin about their own centers and would be mounted on bearings. One scroll plate should be mounted so that it would be possible to adjust the orbiting radius. This configuration would create the required relative orbiting motion with only rotary motion of all components. The plates should be mechanically located in the axial direction rather than attempt to use fluid pressure behind one of the scroll plates to maintain the desired axial clearance. Experience showed that too little pressure behind the plate resulted in low volumetric efficiency and too much pressure lead to galling of the plates. Provision should be made for setting, adjusting, and maintaining the axial clearance between the two scroll plates.

#### MEASUREMENTS

Efforts should be made to measure the pressure in a pocket while the pump is operating. This would verify that the additional discharge ports are large enough and it would also show how fast the pressure in the pocket changes.

Techniques should be evaluated for measuring the axial load on the scroll plates. This would verify the load on the bearings and make it possible to predict bearing life.

#### ACKNOWLEDGMENTS

The authors would like to thank Dr. William J. Levedahl for his initial work in defining the scroll geometry, leakage paths, and possible problems; and for his encouragement and support throughout the program.

APPENDIX A  
SCROLL GEOMETRIC RELATIONSHIPS

The purpose of this appendix is to define the principal equations used in this report and to explain the terms used when working with scroll vanes. It is recommended that readers manipulate these equations and extend them for their individual applications.

From the mathematical definition of an involute, the distance from a point tangent to the generating circle,  $Z$ , is expressed

$$AB = Z = r_g \theta$$

where  $r_g$  is the radius of the generating circle and  $\theta$  is the angle in radians measured from the position at which the involute begins to the position at which the line is perpendicular to the tangent line (Figure 28). The involute can also be thought of as the path described by the end of a string unwinding from a cylinder.

The pitch of the involute is simply

$$\text{pitch} = r_g 2\pi$$

It is emphasized that all measurements of distance are lines that pass tangent to the generating diameter.

The thickness of a vane,  $t$ , is equal to

$$t = r_g \phi$$

where  $\phi$  is the angle in radians between the position at which one edge of the vane begins and the position at which the other edge begins (Figure 29).

In order for a pair of scrolls to be put together, the plates must be positioned a phase angle  $\alpha$  away from each other. This angle can be described

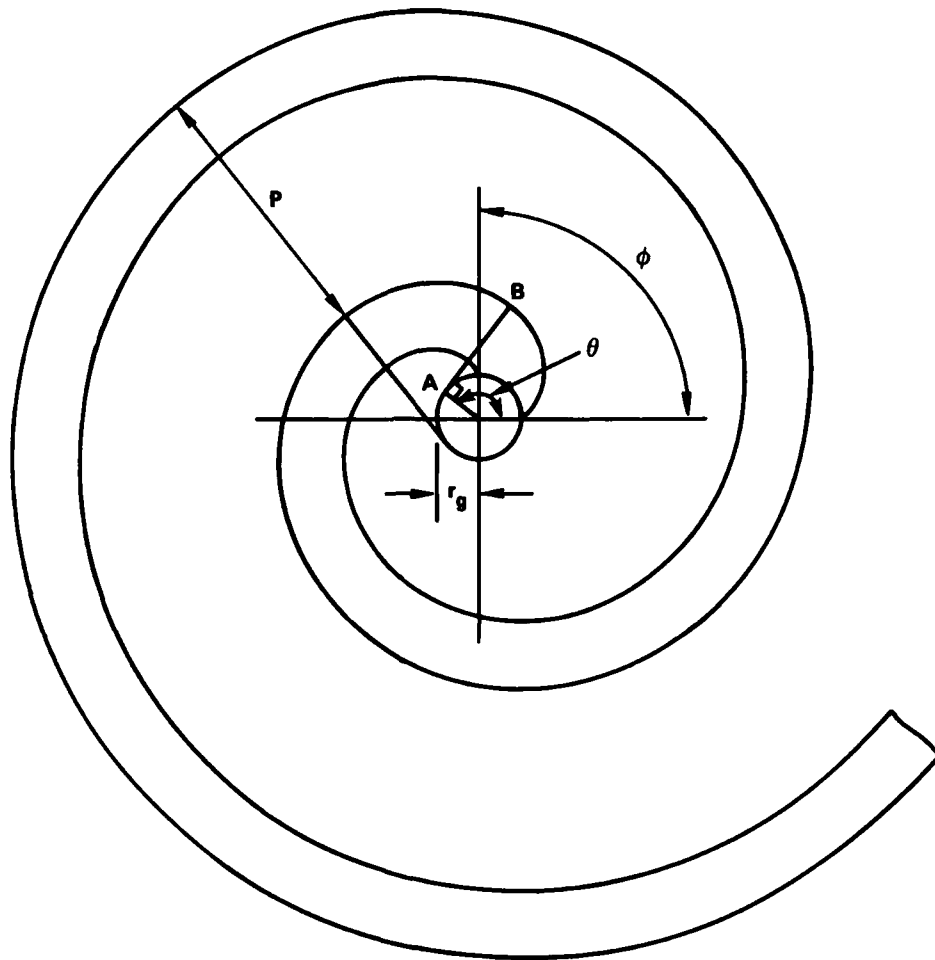


Figure 28 - Basic Geometry.

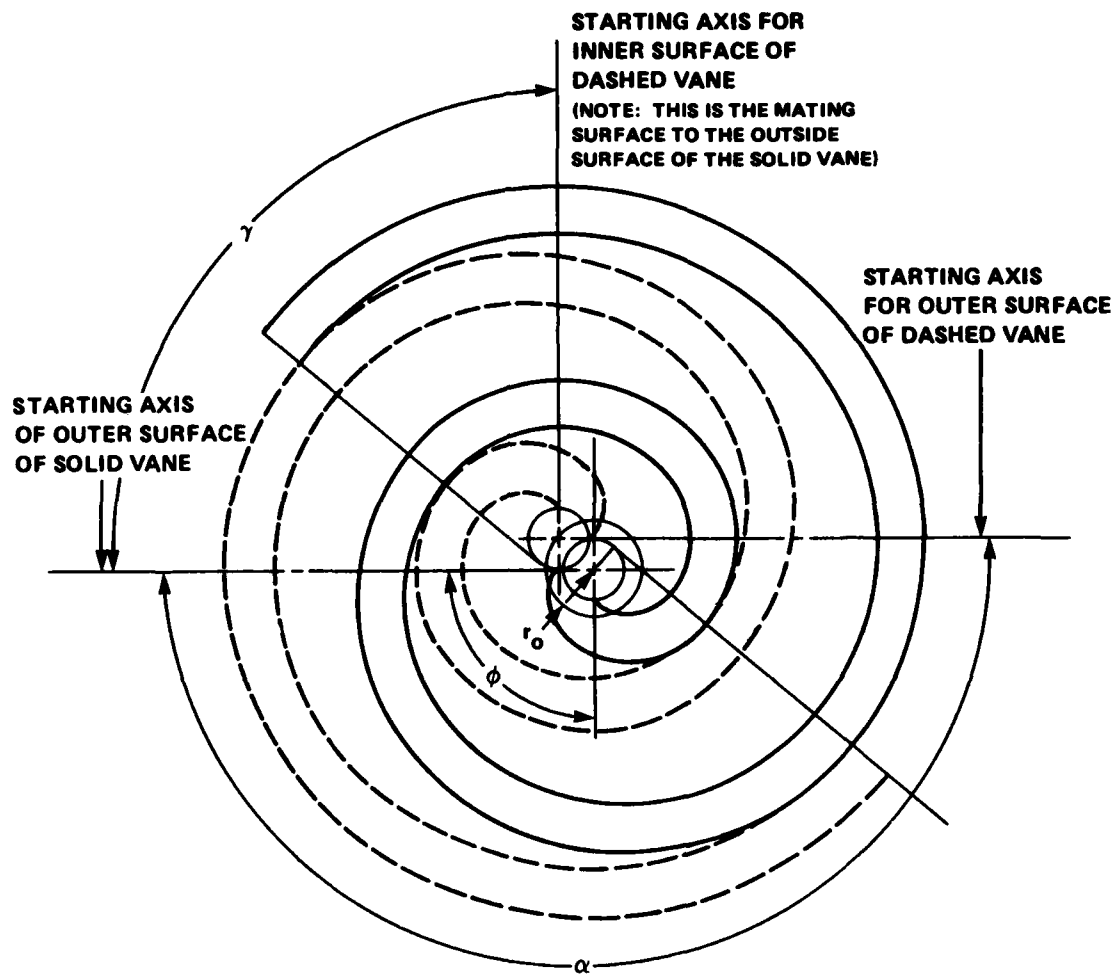


Figure 29 - Scroll Phase Angles

$$\alpha = \frac{\pi}{N_V}$$

where  $N_V$  is the number of vanes on a plate. Referring to Figure 29, there is one vane on each plate. Therefore,  $\alpha = \pi$ .

Another out-of-phase angle that is used is the angle  $\gamma$ , which is the angle between mating scroll surfaces. The mating surfaces that form the seal in the pocket and the angle between them is expressed

$$\gamma = \alpha - \phi$$

The radius that one scroll plate orbits about the center of the other scroll plate is the orbiting radius,  $r_o$ . This is expressed

$$r_o = r_g \gamma$$

#### AREA OF A POCKET

Figure 30 shows the differential piece of involute area. This triangular area can be described

$$\frac{1}{2} (r_g \theta) (r_g \theta d\theta)$$

where  $(r_g \theta)$  is the base of the triangle and  $(r_g \theta d\theta)$  is the height. The area of a bounded involute is the sum of the differential triangular pieces or

$$A_I = \int \frac{1}{2} (r_g \theta) (r_g \theta d\theta)$$

after integrating

$$A_I = \frac{r_g^2}{6} \theta^3 \Big|_{\theta_1}^{\theta_2}$$

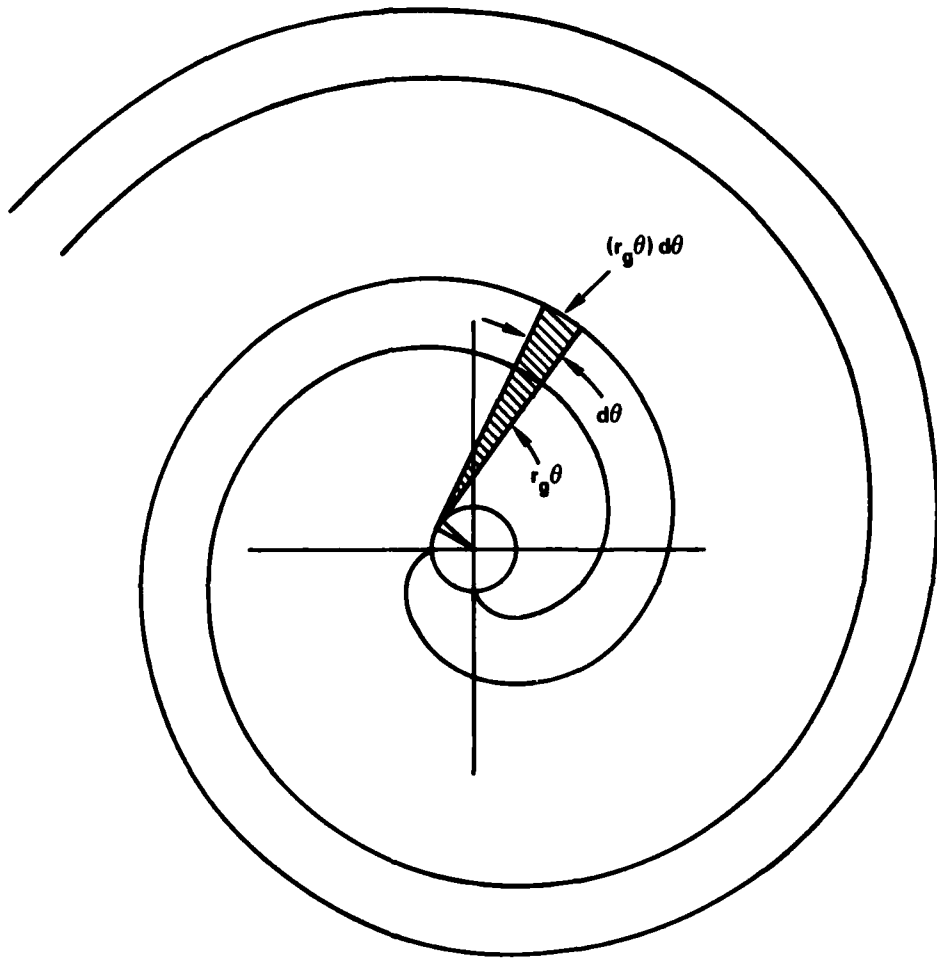


Figure 30 - Differential Involute Area

The area of a pocket bounded by two scroll vanes is the difference between the involute areas contained by the outside and inside sealing surfaces. This is shown in Figure 31 and the symbol convention used for the tangency point angle  $\beta$

$\beta_{IS}$  = inner sealing surface at the start of the pocket

$\beta_{IE}$  = inner sealing surface at the end of the pocket

$\beta_{OS}$  = outer sealing surface at the start of the pocket

$\beta_{OE}$  = outer sealing surface at the end of the pocket

The area of a pocket,  $A_p$ , is then written

$$A_p = \frac{r_g^2}{6} \beta^3 \left| \begin{array}{l} \beta_{OE} \\ - \frac{r_g^2}{6} \beta^3 \\ \beta_{OS} \end{array} \right| \left| \begin{array}{l} \beta_{IE} \\ \beta_{IS} \end{array} \right|$$

which, after substitution, reduces to

$$A_p = \frac{r_g^2}{6} (\beta_{OE}^3 - \beta_{OS}^3 - \beta_{IE}^3 - \beta_{IS}^3)$$

but  $\beta_{OE} = \beta_{IE} + \gamma$

and  $\beta_{OS} = \beta_{IS} + \gamma$


and  $\beta_{IS} = \beta_{IE} - \phi$


After substitution and expansion this reduces to

$$A_p = \frac{\gamma r_g^2}{2} (2\beta_{IE}\phi - \phi^2 + \phi\gamma)$$

and simplifying

$$A_p = \frac{\gamma\phi r_g^2}{2} (2\beta_{IE} - \phi + \gamma)$$

 **AREA SWEEP BY  
INNER SEALING SURFACE**

 **AREA SWEEP BY  
OUTER SEALING SURFACE**

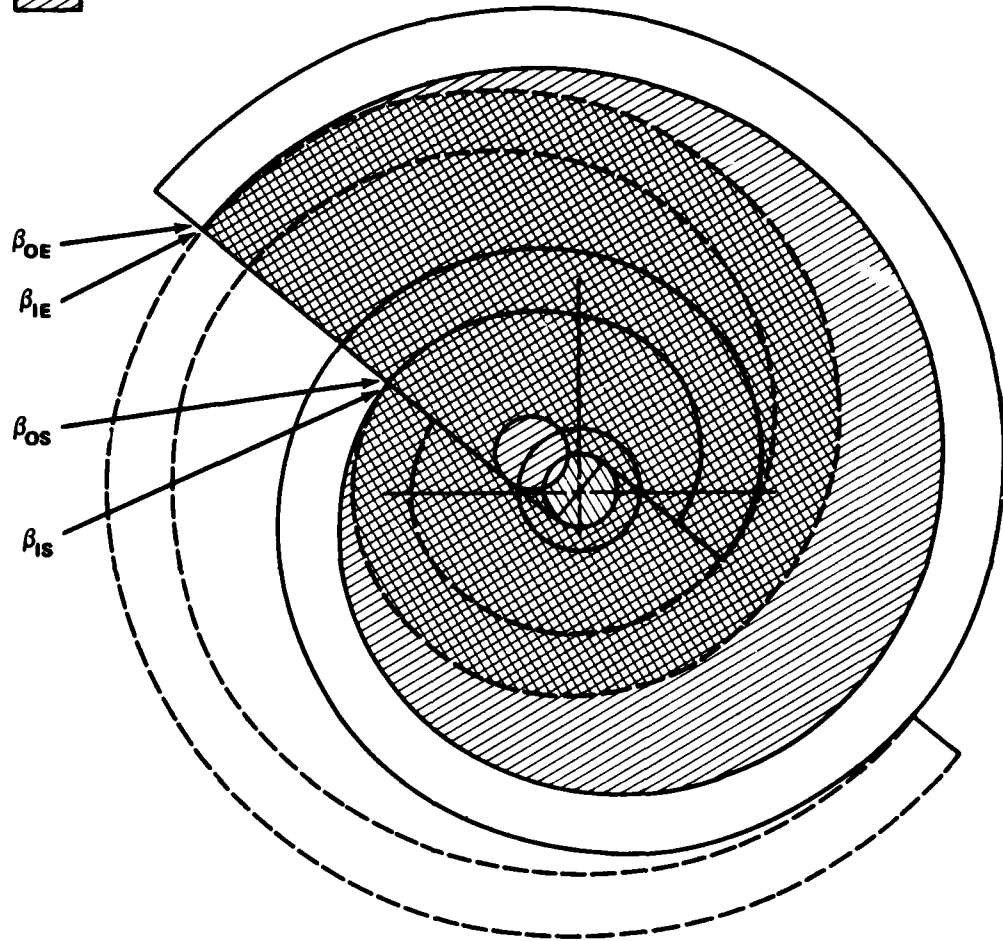


Figure 31 - Area of a Pocket



APPENDIX B  
LEAKAGE PAST THE FLANK OF THE SCROLL VANES

The length of the perimeter of an involute pocket L is expressed

$$L = \int_{\theta_1}^{\theta_2} (r_g \theta) d\theta$$

where  $\theta_1$  and  $\theta_2$  are the end points of the desired length. Integrating and simplifying yields

$$L = r_g \frac{(\theta_2^2 - \theta_1^2)}{2}$$

If  $\theta_2 = \theta_1 + 2\pi$ , then L can be expressed

$$L = 2\pi r_g (\theta_1 + \pi)$$

In this form, the relationship for L is very similar to the equation for the circumference of a circle. The difference is that the radius used in this case is the average of the maximum and minimum lengths Z tangent to the generating circle. Letting

$$X = \theta r_g (\theta_1 - \pi)$$

and

$$R = r_g (\theta_1 - \pi)$$

X becomes

$$X = \theta R$$

Figure 32 shows the shape of a pocket between two scroll vanes for a pocket that has been straightened. In this case, when the gap between the two vanes forming a pocket is a maximum, X is equal to  $\pi R$ .

The gap between the two vanes is

$$\text{gap} = r_o (1 - \cos\theta)$$

Because, in practice, there is a clearance  $Y_o$  between the two sides, this must be included. The total gap between two scroll vane sides Y is expressed

$$Y = Y_o + r_o (1 - \cos\theta)$$

The head loss  $H_L$  through a section of pipe is

$$H_L = \frac{V^2}{2g_c} \frac{\Delta X}{D} f$$

and

$$H_L = \frac{\Delta P}{\rho}$$

where V = velocity through the section  
 $g_c$  = dimensional conversion factor  
D = hydraulic diameter  
f = friction factor  
 $\rho$  = density

Equating and rewriting

$$\frac{dP}{dX} = \frac{\rho V^2}{2g_c} \frac{f}{D} \quad (1)$$

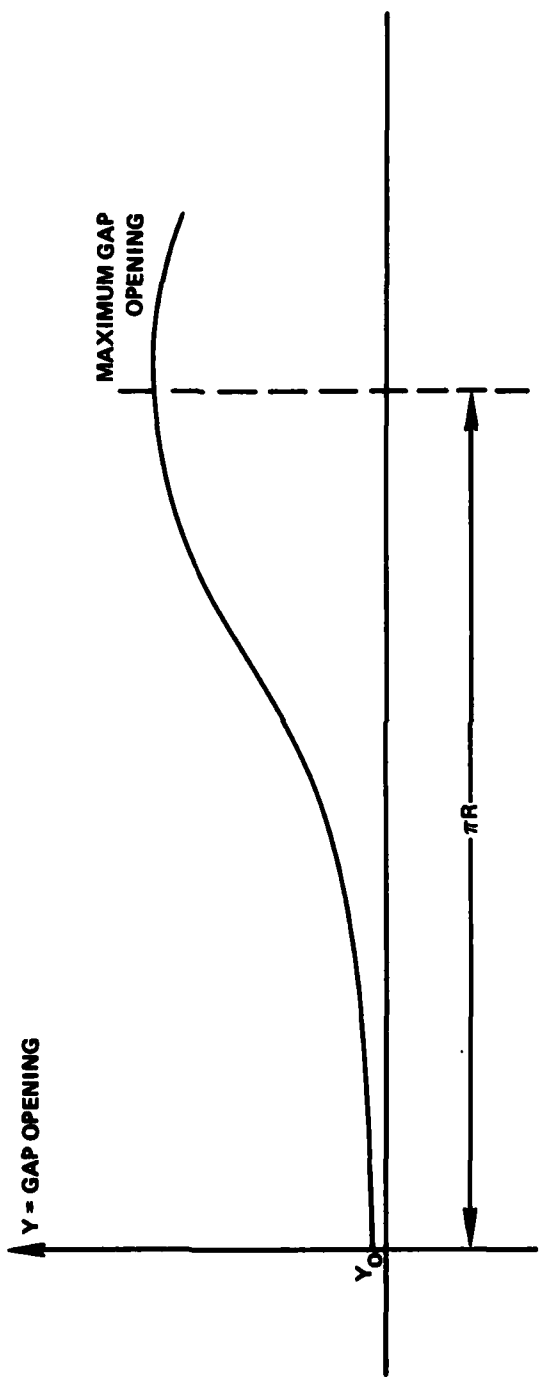


Figure 32 - Gap Between Scroll Sides

Assuming laminar flow with a friction factor approximated by

$$f = \frac{64}{R_e} = \frac{64\mu g_c}{VD\rho}$$

where  $\mu$  is the absolute viscosity and  $R_e$  is the Reynolds Number. Substituting into Equation 1,

$$\frac{dP}{dX} = \frac{32V\mu}{D^2} \quad (2)$$

The hydraulic diameter is four times the ratio of the cross-sectional area to the wetted perimeter. Substituting

$$D = 4 \left( \frac{(YH)}{2(Y+H)} \right)$$

where  $H$  is the height of the scroll vane. Substituting into Equation 2

$$\frac{dP}{dX} = \frac{32V\mu}{\left( \frac{2YH}{Y+H} \right)^2} \quad (3)$$

The flowrate through the gap between the scroll vanes is

$$\dot{\omega} = A_G \rho V = (YH) \rho V$$

where  $A_G$  is the area of the gap. Solving for  $V$  and substituting into Equation 3

$$\frac{dP}{dX} = \frac{32 \left( \frac{\dot{\omega}}{YH\rho} \right) \mu}{\left( \frac{2YH}{Y+H} \right)^2}$$

Simplifying

$$\frac{dP}{dX} = \frac{8\dot{\omega}\mu (Y + H)^2}{\rho Y^3 H^3}$$

Rearranging

$$dP = \frac{8\dot{\omega}\mu (Y + H)^2}{\rho Y^3 H^3} dX$$

Integrating

$$\Delta P = \frac{8\dot{\omega}\mu}{\rho H^3} \int_0^X \frac{(Y + H)^2}{Y^3} dX$$

Recalling the maximum value of Y occurs at  $X = \pi R$ . Putting in these limits and multiplying by  $R/R$ , the equation becomes

$$\Delta P = \frac{8\dot{\omega}\mu R}{\rho H^3} \int_0^{\pi R} \frac{(Y + H)^2}{Y^3} \frac{dX}{R}$$

Recalling

$$X = \theta R$$

Rearranging and taking the derivative

$$d\theta = \frac{dX}{R}$$

Substituting and adjusting the limits

$$\Delta P = \frac{8\dot{\omega}\mu R}{\rho H^3} \int_0^{\pi} \frac{(Y + H)^2}{Y^3} d\theta$$

Rearranging and substituting  $Y = Y_0 + (1 - \cos\theta) r_0$

$$\frac{\Delta P \rho H^3}{8\dot{\omega}\mu R} = \int_0^{\pi} \frac{Y_0 + (1 - \cos\theta) r_0 + H^2}{Y_0 + (1 - \cos\theta) r_0^3} d\theta$$

Simplifying

$$\frac{\Delta P \rho H^3 Y_0}{8\dot{\omega}\mu R} = \int_0^{\pi} \frac{1 + (1 - \cos\theta) \frac{r_0}{Y_0} + \frac{H^2}{Y_0^2}}{1 + (1 - \cos\theta) \frac{r_0}{Y_0}} d\theta$$

Let  $A = r_0/Y_0$  and  $B = H/Y_0$ . From trigonometric identities, the following substitutions will be used

$$\cos\theta = \frac{1 - Z^2}{1 + Z^2}$$

$$d\theta = \frac{2dZ}{1 + Z^2}$$

$$\theta = 2\tan^{-1}Z$$

Making these substitutions and adjusting the limits gives

$$\frac{\Delta P_{\rho H^3 Y_0}}{8\dot{\omega}\mu R} = \int_0^{\infty} \frac{1 + 1 - \frac{1 - Z^2}{1 + Z^2} \frac{A + B}{A}}{1 + 1 - \frac{1 - Z^2}{1 + Z^2} \frac{A + B}{A}} \frac{2dZ}{1 + Z^2}$$

Expanding and simplifying

$$\frac{\Delta P_{\rho H^3 Y_0}}{16\dot{\omega}\mu R} = \int_0^{\infty} \frac{1 + B + Z^2 (1 + 2A + B)}{1 + Z^2 (1 + 2A)} \frac{dZ}{(1 + Z^2)^3}$$

Letting

$$C = 1 + B$$

$$E = 1 + 2A + B$$

$$F = 1 + 2A$$

and substituting

$$\frac{\Delta P_{\rho H^3 Y_0}}{16\dot{\omega}\mu R} = \int_0^{\infty} \frac{(C + Z^2 E)^2 dZ}{(1 + Z^2 F)^3} \quad (4)$$

Using partial fractions to evaluate the integral

$$\frac{(Z^2 E + C)}{(Z^2 F + 1)^3} = \frac{LZ + M}{(Z^2 F + 1)} + \frac{NZ + O}{(Z^2 F + 1)^2} + \frac{PZ + Q}{(Z^2 F + 1)^3}$$

where L, M, N, O, P, and Q are arbitrarily defined constants. From algebra

$$\frac{(Z^2 E + C)}{(Z^2 F + 1)^3} = \frac{(LZ + M)(Z^2 F + 1)^2}{(Z^2 F + 1)(Z^2 F + 1)^2} + \frac{(NZ + O)(Z^2 F + 1)}{(Z^2 F + 1)^2(Z^2 F + 1)} + \frac{PZ + Q}{(Z^2 F + 1)^3}$$

Expanding both sides of this equation and equating coefficients

Order

5	O	=	LF <sup>2</sup>
4	E <sup>2</sup>	=	F <sup>2</sup> M
3	O	=	2FL + NF
2	2EC	=	2FM + OF
1	C <sup>2</sup>	=	M + O + Q

From the fourth-order equation

$$F^2 \neq 0$$

$$M \neq 0$$

Using the above results and inspecting the fifth-order equation

$$L = 0$$

Using the above results and inspecting the third-order equation

$$N = 0$$



Using the above results and inspecting the first-order equation

$$P = 0$$

The fourth-order equation can be solved for M and the result substituted into the second-order equation. This equation can be solved for O and the results substituted into the first-order equation. The results are

$$M = E^2/F^2$$

$$0 = \frac{2EFC - 2E^2}{F^2}$$

$$Q = \frac{(E^2 + 2EFC - 2E^2)}{F^2} - C^2$$

Recalling

$$\frac{(Z^2E + C)^2}{(Z^2F + 1)^3} = \frac{LZ + M}{Z^2F + 1} + \frac{NZ + O}{(Z^2F + 1)^2} + \frac{PZ + Q}{(Z^2F + 1)^3}$$

Substituting the results from the partial fractions and integrating

$$\int_0^{\infty} \frac{(Z^2E + C)^2}{(Z^2F + 1)^3} dZ = \int_0^{\infty} \frac{E^2 dZ}{F^2 (1 + Z^2F)} + \int_0^{\infty} \frac{(2EFC - 2E^2) dZ}{F^2 (1 + Z^2F)^2} + \int_0^{\infty} \frac{(C^2F^2 - E^2 - 2EFC + 2E^2) dZ}{F^2 (1 + Z^2F)^3} \quad (5)$$

The components from Equation 5 are assigned as follows:

$$\text{Component A: } \int_0^{\infty} \frac{(E^2 dZ)}{F^2 (1 + Z^2 F)}$$

$$\text{Component B: } \int_0^{\infty} \frac{(2EFC - 2E^2) dZ}{F^2 (1 + Z^2 F)^2}$$

$$\text{Component C: } \int_0^{\infty} \frac{(C^2 F^2 - E^2 - 2EFC + 2E^2) dZ}{F^2 (1 + Z^2 F)^3}$$

Integrating Component A and reducing it gives

$$J \frac{1}{F} \tan^{-1} (Z\sqrt{F}) \Bigg|_0^{\infty}$$

where  $J = E^2/F^2$ .

Integrating Component B and reducing it gives

$$S \left( \frac{Z}{2(1 + FZ^2)} + \frac{1}{2} \left( \frac{1}{\sqrt{F}} \tan^{-1} (Z\sqrt{F}) \right) \right) \Bigg|_0^{\infty}$$

where  $S = \frac{2(EFC - 2E^2)}{F^2}$ .

Integrating Component C and reducing it gives

$$T \left( \frac{Z}{4 (1 + FZ^2)^2} + \frac{3}{4} \left( \frac{Z}{2 (1 + FZ^2)} + \frac{1}{2} \left( \frac{1}{\sqrt{F}} \tan (Z \sqrt{F}) \right) \right) \right) \Bigg|_0^{\infty}$$

$$\text{where } T = \frac{(F^2 C^2 - E^2 - 2EFC + 2E^2)}{F^2} .$$

Letting

$$I = \frac{1}{\sqrt{F}} \left\{ \tan^{-1} (Z \sqrt{F}) \right\}$$

$$II = \frac{Z}{2 (1 + FZ^2)}$$

$$III = \frac{Z}{4 (1 + FZ^2)^2}$$

Components A, B, and C of Equation 5 become

$$\text{Component A} = J I \Bigg|_0^{\infty}$$

$$\text{Component B} = S \left( II + \frac{1}{2} I \right) \Bigg|_0^{\infty}$$

$$\text{Component C} = T \left( III + \frac{3}{4} \left( II + \frac{1}{2} I \right) \right) \Bigg|_0^{\infty}$$

To evaluate I, substitute  $Z = \tan \frac{\theta}{2}$  with limits  $0 \rightarrow \pi$

$$I = \frac{1}{\sqrt{F}} \left( \tan^{-1} \left( \tan \frac{\theta}{2} \sqrt{F} \right) \right) \Big|_0^\pi$$

From power series

$$I = \frac{\pi}{2\sqrt{F}}$$

Evaluating II, substitute for Z again

$$II = \frac{\tan \frac{\theta}{2}}{2 \left( 1 + F \left( \tan \frac{\theta}{2} \right)^2 \right)} \Big|_0^\pi$$

Evaluating the limits

$$II = 0$$

Evaluating III, substitute for Z again

$$III = \frac{\tan \frac{\theta}{2}}{4 \left( 1 + F \left( \tan \frac{\theta}{2} \right)^2 \right)} \Big|_0^\pi$$

Evaluating the limits

$$III = 0$$

Recalling Equation 4 and substituting the results of Equation 5 (Components A, B, and C)

$$\frac{\Delta P \rho H^3 Y_o}{16 \dot{\omega} \mu R} = JI + S \left( II + \frac{1}{2} I \right) + T \left( III + \frac{3}{4} \left( II + \frac{1}{2} I \right) \right)$$

Substituting the values for I, II, and III yields

$$\frac{\Delta P \rho H^3 Y_o}{16 \dot{\omega} \mu R} = \frac{J\pi}{2 F} + \left( \frac{S}{2} \right) \left( \frac{\pi}{2 \sqrt{F}} \right) + \frac{3T}{8} \left( \frac{\pi}{2 \sqrt{F}} \right)$$

Simplifying

$$\frac{\Delta P \rho H^3 Y_o}{16 \dot{\omega} \mu R} = \frac{\pi}{2 F} \left( J + \frac{S}{2} + \frac{3T}{8} \right)$$

Substituting the values for J, S, and T this reduces to

$$\frac{\Delta P \rho H^3 Y_o}{\dot{\omega} \mu R} = \frac{\pi}{F^{2.5}} \left( (FC (2E + 2FC)) + 3E^2 \right)$$

Solving for  $\dot{\omega}$

$$\dot{\omega} = \frac{\Delta P \rho H^3 Y_o F^{2.5}}{\pi \mu R \left( (FC (2E + 3FC)) + 3E^2 \right)}$$

where  $A = r_o / Y_o$

$B = H / Y_o$

$C = 1 + B$

$$E = 1 + 2A + B$$

$$F = 1 + 2A$$

Although the result is quite long, further substitution does not produce a simpler form.

#### REFERENCES

1. Bein, T., "Discharge Ports for Mechanisms with Involute Shaped Vanes," Patent Application, Navy Case No. 62,016, filed September 1978.
2. Stepanoff, A. J., "Centrifugal and Axial Flow Pumps," John Wiley and Sons, Inc., New York (1957), pp. 182-186.
3. Thelen, W. and T. Bein, "Relative Orbiting Motion by Synchronously Rotating Scroll Members," Patent Application, Navy Case No. 62,085, filed March 1978.

INITIAL DISTRIBUTION

Copies

4 NAVSEA  
 1 SEA 05D  
 1 SEA 5321/J. Corso  
 2 SEA 99612  
 12 DTIC

CENTER DISTRIBUTION

Copies	Code	Name
1	011	Dr. Jewel
1	2702	W. Levedahl
1	272	E. Quandt
6	2706	J. Harrison
2	2722	J. Ward
10	2722	H. Skruch
10	5211.1	Repts Dist
1	522.1	Unclass Lib (C)
1	522.2	Unclass Lib (A)
2	5231	Office Services



